
WHY FLATNESS CORRELATES WITH GENERALIZATION FOR DEEP NEURAL NETWORKS

Shuofeng Zhang¹ Isaac Reid² Guillermo Valle Pérez¹ Ard Louis¹

Abstract

The intuition that local flatness of the loss landscape is correlated with better generalization for deep neural networks (DNNs) has been explored for decades, spawning many different local flatness measures. Here we argue that these measures correlate with generalization because they are local approximations to a global property, the volume of the set of parameters mapping to a specific function. This global volume is equivalent to the Bayesian prior upon initialization. For functions that give zero error on a test set, it is directly proportional to the Bayesian posterior, making volume a more robust and theoretically better grounded predictor of generalization than flatness. Whilst flatness measures fail under parameter re-scaling, volume remains invariant and therefore continues to correlate well with generalization. Moreover, some variants of SGD can break the flatness-generalization correlation, while the volume-generalization correlation remains intact.

1. Introduction

Among the most important theoretical questions in the field of deep learning are: 1) What characterizes functions that exhibit good generalization?, and 2) Why do overparameterized deep neural networks (DNNs) converge to this small subset of functions that do not overfit? Perhaps the most popular hypothesis is that good generalization performance is linked to flat minima. In pioneering works, Hinton & van Camp (1993); Hochreiter & Schmidhuber (1997), the minimum description length (MDL) principle (Rissanen, 1978) was invoked to argue that since flatter minima require less

information to describe, they should generalize better than sharp minima. Most measures of flatness approximate the local curvature of the loss surface, typically defining flatter functions to be those with smaller values of the Hessian eigenvalues (Keskar et al., 2016; Wu et al., 2017; Zhang et al., 2018; Sagun et al., 2016; Yao et al., 2018).

Another commonly held belief is that stochastic gradient descent (SGD) is itself biased towards flatter minima, and that this inductive bias helps explain why DNNs generalize so well (Keskar et al., 2016; Jastrzebski et al., 2018; Wu et al., 2017; Zhang et al., 2018; Yao et al., 2018; Wei & Schwab, 2019; Maddox et al., 2020). For example Keskar et al. (2016) developed a measure of flatness that they found correlated with improved generalization performance with decreasing batch size, suggesting that SGD is itself biased towards flatter minima. We note that others (Goyal et al., 2017; Hoffer et al., 2017; Smith et al., 2017; Mingard et al., 2020) have argued that the effect of batch size can be compensated by changes in learning rate, complicating some conclusions from Keskar et al. (2016). Nevertheless, the argument that SGD is somehow itself biased towards flat minima remains widespread in the literature.

In an important critique of local flatness measures, Dinh et al. (2017) pointed out that DNNs with ReLU activation can be re-parameterized through an “alpha scaling” transformation.

$$T_\alpha : (\mathbf{w}_1, \mathbf{w}_2) \mapsto (\alpha \mathbf{w}_1, \alpha^{-1} \mathbf{w}_2) \quad (1)$$

where \mathbf{w}_1 are the weights between an input layer and a single hidden layer, and \mathbf{w}_2 are the weights between this hidden layer and the outputs. This transformation can be extended to any architecture having at least one single rectified network layer. The function that the DNN represents, and thus its generalization, is invariant under alpha scaling transformations, but the derivatives w.r.t. parameters, and therefore many flatness measures used in the literature, can be changed arbitrarily. *Ergo*, the correlation between flatness and generalization can be arbitrarily changed.

Several recent studies have attempted to find “scale invariant” flatness metrics (Petzka et al., 2019; Rangamani et al., 2019; Tsuzuku et al., 2019). The main idea is to multiply layer-wise Hessian eigenvalues by a factor of $\|\mathbf{w}_i\|^2$, which renders the metric immune to layer-wise re-parameterization.

¹Rudolf Peierls Centre for Theoretical Physics, Department of Physics, University of Oxford, Oxford, United Kingdom ²Hertford college, University of Oxford, Oxford, United Kingdom. Correspondence to: Shuofeng Zhang <shuofeng.zhang@physics.ox.ac.uk>, Ard Louis <ard.louis@physics.ox.ac.uk>.

While these new metrics look promising experimentally, they are only scale-invariant when the scaling is layer-wise. Other methods of rescaling (e.g. neuron-wise rescaling) can still change the metrics, so this general problem remains unsolved.

In this paper we examine the link between measures of flatness and generalization in light of the ‘‘volume’’ $V(f)$ of a function f , defined as a weighted integral over all parameters for which the DNN maps to f . Intuitively, we expect local flatness measures to typically be smaller (flatter) for systems with larger volumes. Nevertheless, there may be regions of parameter space where local derivatives are very large. These are probed, for example, with the alpha-scaling transformation. Volumes are invariant to alpha-scaling re-parameterization.

In the context of supervised learning with training to zero error on a training set, we show that the volume is directly proportional to the Bayesian posterior. Following [Mingard et al. \(2020\)](#) we therefore expect $\log(V(f))$ to correlate linearly with generalization performance. We show empirically that volume is indeed a robust predictor of generalization. By contrast, while the flatness-generalization correlation works for vanilla SGD, it can be broken, for example, by alpha scaling, or else in some cases by the use of certain SGD variants such as Adam ([Kingma & Ba, 2014](#)) or entropy-SGD ([Chaudhari et al., 2019](#)).

2. Definitions and notation

2.1. Supervised learning

For a typical supervised learning problem, the *inputs* live in an input domain \mathcal{X} , and the *outputs* belong to an output space \mathcal{Y} . For a *data distribution* \mathcal{D} on the set of input-output pairs $\mathcal{X} \times \mathcal{Y}$, the *training set* S is a sample of m input-output pairs sampled i.i.d. from \mathcal{D} , $S = \{(x_i, y_i)\}_{i=1}^m \sim \mathcal{D}^m$, where $x_i \in \mathcal{X}$ and $y_i \in \mathcal{Y}$. The output of a DNN on an input x_i is denoted as \hat{y}_i . Typically a DNN is trained by minimising a *loss function* $L : \mathcal{Y} \times \mathcal{Y} \rightarrow \mathbb{R}$, which measures differences between the output $\hat{y} \in \mathcal{Y}$ and the observed output $y \in \mathcal{Y}$, by assigning a score $L(\hat{y}, y)$ which is typically zero when they match, and positive when they don’t match. DNNs are typically trained by using an optimization algorithm such as SGD to minimize the loss function on a training set S . The generalization performance of the DNN is then measured on a *test set* $E = \{(x'_i, y'_i)\}_{i=1}^{|E|} \sim \mathcal{D}^{|E|}$. For classification problems, the *generalization error* is defined as $\epsilon(E) = \frac{1}{|E|} \sum_{x'_i \in E} \mathbb{1}[\hat{y}_i \neq y'_i]$, where $\mathbb{1}$ is the standard indicator function which is one when its input is true, and zero otherwise.

2.2. Flatness measures

Perhaps the most natural way to measure the flatness of minima is to consider the eigenvalue distribution of the Hessian $H_{ij} = \partial^2 L(\mathbf{w}) / \partial w_i \partial w_j$ once the learning process has converged (typically to a zero training error solution). Sharp minima are characterized by a significant number of large positive eigenvalues λ_i in the Hessian, while flat minima have numerous small eigenvalues. Some care must be used in this interpretation because it is widely thought that DNNs converge to stationary points that are not true minima, leading to negative eigenvalues and complicating their use in measures of flatness. Typically, only a subset of the positive eigenvalues are used ([Wu et al., 2017](#); [Zhang et al., 2018](#)).

Hessians are typically very expensive to calculate. For this reason [Keskar et al. \(2016\)](#) introduced a computationally more tractable measure called ‘‘sharpness’’:

Definition 2.1 (Sharpness). Given parameters \mathbf{w}' within a box in parameter space \mathcal{C}_ϵ with sides of length $\epsilon > 0$, centered around a minimum of interest at parameters \mathbf{w} , the sharpness of the loss $L(\mathbf{w})$ at \mathbf{w} is defined as:

$$\text{sharpness} := \frac{\max_{\mathbf{w}' \in \mathcal{C}_\epsilon} (L(\mathbf{w}') - L(\mathbf{w}))}{1 + L(\mathbf{w})} \times 100.$$

In the limit of small ϵ , the sharpness can be related to the spectral norm of the Hessian ([Dinh et al., 2017](#)):

$$\text{sharpness} \approx \frac{\|(\nabla^2 L(\mathbf{w}))\|_2 \epsilon^2}{2(1 + L(\mathbf{w}))} \times 100.$$

2.3. Functions and volume

We first clarify how we *represent* functions in the rest of paper, using classification as an example:

Definition 2.2 (Representation of Functions). Consider a DNN, a training set $S = \{(x_i, y_i)\}_{i=1}^m$ and test set $E = \{(x'_i, y'_i)\}_{i=1}^{|E|}$. We *represent* the function $f(\mathbf{w})$ for a set of DNN parameters \mathbf{w} as a string of length $(|S| + |E|)$, where the values are the labels \hat{y}_i and \hat{y}'_i that the DNN produces on the concatenation of training and testing inputs.

For example, for binary classification, the function is represented as a binary string of length $|S| + |E|$. In some cases, such as the Boolean system described in [Valle-Pérez et al. \(2018\)](#) and treated in section 5.1, this representation is complete because it is feasible to enumerate all possible inputs. However, for real-life data distributions the number of all possible inputs is hyper-astronomically large, and so the definition above is usually a coarse-grained one based on the user’s choice of S and E . For example, for MNIST ([LeCun et al., 1998](#)), all inputs would include the set of 28x28 integer matrices whose entries take values from 0-255, which gives 256^{784} possible inputs.

The link between functions and a DNN is described by the:

Definition 2.3 (Parameter-function map). Consider a parameterized supervised model, and let the input space be \mathcal{X} and the output space be \mathcal{Y} . The space of functions the model can express is a set $\mathcal{F} \subseteq \mathcal{Y}^{|\mathcal{X}|}$. If the model takes parameters within a set $W \subseteq \mathbb{R}^n$, then the parameter-function map \mathcal{M} is defined as

$$\begin{aligned} \mathcal{M} : W &\rightarrow \mathcal{F} \\ \mathbf{w} &\mapsto f(\mathbf{w}). \end{aligned}$$

First defined by Valle-Pérez et al. (2018), the parameter-function map serves as a bridge between a parameter searching algorithm (e.g. SGD) and the behaviour of a DNN in function space. In this context we also define the:

Definition 2.4 (Neutral space). For a model defined in Definition 2.3, and a given function f , the neutral space $\mathcal{N}_f \subseteq W$ is defined as

$$\mathcal{N}_f := \{\mathbf{w} \in W : \mathcal{M}(\mathbf{w}) = f\}.$$

The nomenclature comes from genotype-phenotype maps in the evolutionary literature (Manrubia et al., 2020), where the space is typically discrete, and a neutral set refers to all genotypes that map to the same phenotype.

If parameters are bounded, then defining a volume by integrating over the neutral space is straightforward. For unbounded parameters, where the neutral spaces may be infinite, we can turn to a probabilistic interpretation:

Definition 2.5 (Volume of a function). Given a prior parameter distribution $P_w(\mathbf{w})$ over the parameters, the *volume of function* f can be defined as:

$$V(f) := \int \mathbb{1}[\mathcal{M}(\mathbf{w}) = f] P_w(\mathbf{w}) d\mathbf{w}. \quad (2)$$

$V(f)$ can be interpreted as the probability that the DNN expresses function f upon random sampling of initial parameters with a prior parameter distribution $P_w(\mathbf{w})$ which acts as a measure on the space. Such prior parameter distributions are typically used at initialization, in which case $V(f)$ can be interpreted as the prior probability $P(f)$ that a DNN represents the function f at initialization.

2.4. Link between volume and the Bayesian posterior

Due to their high expressivity, DNNs are typically trained to zero training error on training set S . For this case, the volume can be naturally interpreted within the Bayesian picture of Valle-Pérez et al. (2018); Mingard et al. (2020). If functions are conditioned on zero error on S , this leads to a simple 0-1 *likelihood* $P(S|f)$, indicating whether the data is consistent with the function. Bayesian inference can be used to calculate a Bayesian *posterior probability* $P_B(f|S)$

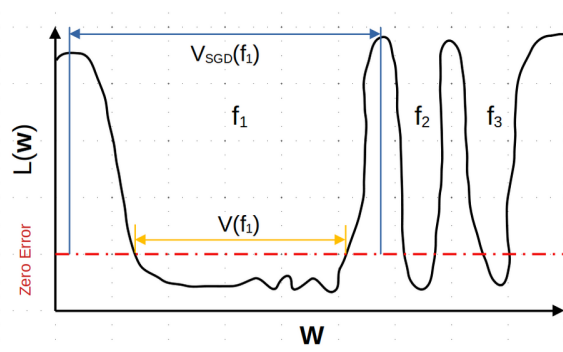


Figure 1. Schematic loss landscape for three functions that have zero-error on the training set. It illustrates how the relative sizes of the volumes of their basins of attraction $V_{\text{SGD}}(f_i)$ correlate with the volumes $V(f_i)$ of the basins, and that, on average, larger $V(f_i)$ implies flatter functions, even if flatness can vary locally. Note that the loss $L(\mathbf{w})$ can vary within a region where the DNN achieves zero classification error on S .

for each f by conditioning on the data according to Bayes rule. Formally, if $S = \{(x_i, y_i)\}_{i=1}^m$ corresponds to the set of training pairs, then

$$P_B(f|S) = \begin{cases} P(f)/P(S) \propto V(f) & \text{if } \forall i, f(x_i) = y_i \\ 0 & \text{otherwise.} \end{cases}$$

where $P(f)$ is the Bayesian prior, which is equivalent to our definition of volume $V(f)$ above, and $P(S)$ is called the *marginal likelihood* or *Bayesian evidence*. If we define, similarly to definition 2.4, the training set neutral space \mathcal{N}_S as all parameters that lead to functions that give zero training error on S , then $P(S) = \int_{\mathcal{N}_S} P_w(\mathbf{w}) d\mathbf{w}$. In other words, it is the total prior probability (or volume) of all functions compatible with the training set (Valle-Pérez et al., 2018; Mingard et al., 2020) S . Since $P(S)$ is constant for a given S , $P_B(f|S) \propto P(f) = V(f)$ for all f consistent with that S . In other words, for fixed S , the volumes and priors for functions that give zero error on the training set are directly proportional to the Bayesian posterior.

3. The correlation between volume and generalization

This link between the volume and the posterior is important, because it was shown empirically in (Mingard et al., 2020) that

$$P_B(f|S) \approx P_{\text{SGD}}(f|S), \quad (3)$$

where $P_{\text{SGD}}(f|S)$ is the probability that a DNN trained with SGD converges on function f , when trained to zero error on S . In other words, to first order, SGD finds functions with a probability predicted by the Bayesian posterior, and thus with probabilities directly proportional to $V(f)$. The authors

traced this behaviour to the geometry of the loss-landscape. Quite general arguments from algorithmic information theory (AIT) (Valle-Pérez et al., 2018) as well as direct calculations (Mingard et al., 2019) predict that the volumes of functions should vary over many orders of magnitude. When this is true, a mechanism, also identified previously in evolutionary dynamics where it is called the arrival of the frequent (Schaper & Louis, 2014), is at play. It is illustrated in fig. 1: the relative sizes of the basins of attraction $V_{SGD}(f)$, defined as the set of initial parameters for which a DNN converges to a certain function f , is proportional, to first order, to those of the volumes $V(f)$. To second order there are, of course, many other features of a search method and a landscape that affect what functions a DNN converges on, but when the volumes vary by so many orders of magnitude then to first order $P_{SGD}(f) \approx P_B(f|S) \propto V(f)$.

This result runs counter to widely held beliefs that there is something special about SGD that explains DNN generalization. There is plenty of evidence that SGD is an excellent optimizer for DNNs. By contrast, the evidence that it also plays a determining role in explaining the conundrum of why DNNs generalize in the overparameterised regime, where classical learning theory predicts that they will overfit, is much weaker than generally acknowledged. The empirical results from Mingard et al. (2020), showing that $P_B(f|S) \approx P_{SGD}(f)$, strongly suggest that SGD does not, to first order, explain why DNNs generalize so well in the overparameterized regime. Instead, the answer to this question must be found in properties of the posterior $P_B(f|S)$, or more generally, the parameter-function map (Valle-Pérez et al., 2018). Of course hyperparameter tuning of SGD can improve generalization, but these changes are typically smaller second order effects which may vary from system to system and do not provide an overall explanation of the generalization conundrum.

Given that the volume of a function helps predict how likely SGD is to converge on that function, we can next ask how the volume correlates with generalization. Perhaps the simplest argument is that if DNNs trained to zero error are known to generalize well on unseen data, then the probability of converging on functions that generalize well must be high. The volumes of these functions must be larger than the volumes of functions that do not generalize well.

Can we do better than this rather simplistic argument? One way forward is empirical. Mingard et al. (2020) showed that $\log(P_B(f|S))$ correlates quite tightly with generalization error. These authors also made a theoretical argument based on the Poisson-Binomial nature of the error distribution to explain this log-linear relationship, but this approach needs further work.

The best performing predictor in the literature for generalization performance is the marginal likelihood PAC-Bayes

bound from (Valle-Pérez et al., 2018; Valle-Pérez & Louis, 2020). It is relatively tight (non-vacuous), and can capture important trends in generalization performance with training set size (learning curves), data complexity, and architecture choice. However, the prediction uses the marginal likelihood $P(S)$ defined through a sum over all functions that produce zero error on the training set. Here we are interested in properties of a single function.

One way forward is to use a simple nonuniform bound which to the best of our knowledge was first put forward in (McAllester, 1998) as a preliminary theory to the full PAC-Bayes theorems. For any countable function space \mathcal{F} , any distribution P , and for any selection of a training set S of size m under probability distribution \mathcal{D} , it can be proven that for all functions f that give zero training error:

$$\forall \mathcal{D}, \mathbf{P}_{S \sim \mathcal{D}^m} \left[\epsilon_{S,E}(f) \leq \frac{\ln \frac{1}{P(f)} + \ln \frac{1}{\delta}}{m} \right] \geq 1 - \delta \quad (4)$$

for $\delta \in (0, 1)$. Here we consider a space $\mathcal{F}_{S,E}$ of functions with all possible outputs on the inputs of a specific E and zero error on a specific S ; $\epsilon_{S,E}(f)$ is the error measured on E , given S . This error will converge to the true generalization error on all possible inputs as $|S|$ increases. Valle-Pérez & Louis (2020) showed this bound has an optimal average generalization error when $P(f)$ mimics the probability distribution over functions of the learning algorithm. If $P_{SGD}(f) \approx P_B(f|S) \propto V(f)$, then the best performance of the bound is approximately when $P(f)$ in eq. (4) is the Bayesian prior, which is equal to $V(f)$. Thus this upper bound on $\epsilon_{S,E}(f)$ scales as $-\log(V(f))$.

4. Flatness, volume and generalization

The intuition that larger volume correlates with greater flatness is common in the literature, see e.g. Hochreiter & Schmidhuber (1997); Wu et al. (2017). If volume correlates with generalization, then so will flatness. Nevertheless, local flatness may still vary significantly across a neutral space. For example Izmailov et al. (2018) show explicitly that even in the same basin of attraction, there can be flatter and sharper regions. We illustrate this point schematically in fig. 1, where one function clearly has a larger volume and on average smaller derivatives of the loss w.r.t. the parameters than the others, and so is flatter on average. But, there are also local areas within the zero-error region where this correlation does not hold. One of the main hypotheses we will test in this paper is that the correlation between flatness and generalization can be broken even when the generalization-volume correlation remains robust.

5. Experimental Results

5.1. Volume - flatness correlation for Boolean system

We first study a model system for Boolean functions of size $n = 7$, which is small enough to directly measure the volume by sampling (Valle-Pérez et al., 2018). There are $2^7 = 128$ possible binary inputs. Since each input is mapped to a single binary output, there are $2^{128} = 3.4 \times 10^{34}$ possible functions f . It is only practically possible to sample $V(f)$ because the prior $P(f)$ is highly biased (Valle-Pérez et al., 2018; Mingard et al., 2019), meaning a subset of functions have priors much higher than average. For a fully connected network (FCN) with two hidden layers of 40 ReLU units each (which was found to be sufficiently expressive to represent almost all possible functions) we empirically determine $V(f)$ using 10^8 random samples of the weights \mathbf{w} over an initial Gaussian parameter distribution $P_w(\mathbf{w})$ with standard deviation $\sigma_w = 1.0$ and offset $\sigma_b = 0.1$.

We also train our network with SGD using the same initialization and record the top-1000 most commonly appearing output functions with zero training error on all 128 outputs, and then evaluate the sharpness using definition 2.1 with an $\epsilon = 10^{-4}$. For the maximization process in calculating sharpness, we run SGD for 10 epochs and make sure the max value ceases to change. As fig. 2 demonstrates, sharpness and volume correlate relatively well; fig. S2 in the appendix shows a very similar correlation for the the spectral norm of the Hessian. Note that since we are studying the function on the complete input space, it is not meaningful to speak of correlation with generalization. However, since for this system the volume $V(f)$ is known to correlate with generalization (Mingard et al., 2020), the correlation in fig. 2 also implies that these flatness measures will correlate with generalization, at least for these high $P(f)$ functions.

5.2. Volume, flatness and generalization for MNIST and CIFAR-10

We next study the correlation between generalization, flatness and volume on the real world datasets MNIST (LeCun et al., 1998) and CIFAR-10 (Krizhevsky et al., 2009).

Because we need to run many different experiments, and measurements of volume and flatness are computationally expensive, we simplify the problem by binarizing MNIST (one class is 0-4, the other is 5-9) and CIFAR-10 (we only study two categories out of ten: cars and cats). Also, our training sets are relatively small (500/5000 for MNIST/CIFAR-10, respectively) but we have checked that our overall results are not affected by these more computationally convenient choices. In Appendix fig. S18 we show results for MNIST with $|S| = 10000$.

We use two DNN architectures: a relatively small vanilla two hidden-layer FCN with 784 inputs and 40 ReLU units

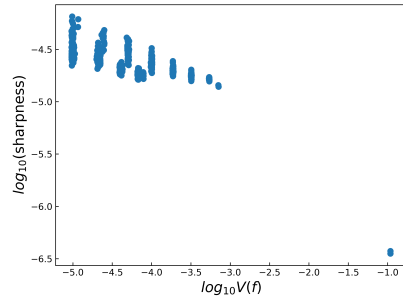


Figure 2. **The correlation between flatness/sharpness and volume for the $n = 7$ Boolean system.** The functions are defined on the full space of 128 possible inputs. The volumes $V(f)$ are shown for the 1000 most frequently found functions by SGD from random initialization for a two hidden layer FCN, and correlate well with $\log(\text{sharpness})$. The largest volume/lowest sharpness function is the trivial one of all 0s or all 1s. An additional feature is two offset bands caused by a flatness discontinuity of Boolean functions. Most functions shown are mainly 0s or mainly 1s, and the two bands correspond to an even or odd number of outliers (e.g. 1’s when the majority is 0s).

in each hidden layer each, and also Resnet-50 (He et al., 2016), a 50-layer deep convolutional neural network, which is much closer to a state of the art (SOTA) system.

We measure the flatness on cross-entropy (CE) loss at the epoch where SGD first obtains zero training error. Because the Hessian is so expensive to calculate, we mainly use the sharpness measure (definition 2.1) which is proportional to the Frobenius norm of the Hessian. The final error is measured in the standard way, after applying a sigmoid to the last layer to binarize the outputs.

To measure the volume, we use the Gaussian processes (GPs) to which these networks reduce in the limit of infinite width (Lee et al., 2017; Matthews et al., 2018; Novak et al., 2018b). As demonstrated in Mingard et al. (2020), GPs can be used to approximate the Bayesian posteriors $P_B(f|S)$ for finite width networks. For a given S and E , we use GPs to directly calculate the volume for the $|S| + |E|$ input-output pairs that define the function f . For further details, we refer to the original papers and to appendix A.

In order to generate functions f with zero error on the training set S , but with diverse generalization performance, we use the attack-set trick from Wu et al. (2017). In addition to training on S , we add an attack set A made up of incorrectly labelled data. We train on both S and A , so that the error on S is zero but the generalization performance on a test set E is reduced. The larger A is w.r.t. S , the worse the generalization performance. As can be seen in fig. 3(a)-(c), this process allows us to significantly change the generalization performance. The correlation with between volume and generalization error is excellent over this range, as expected

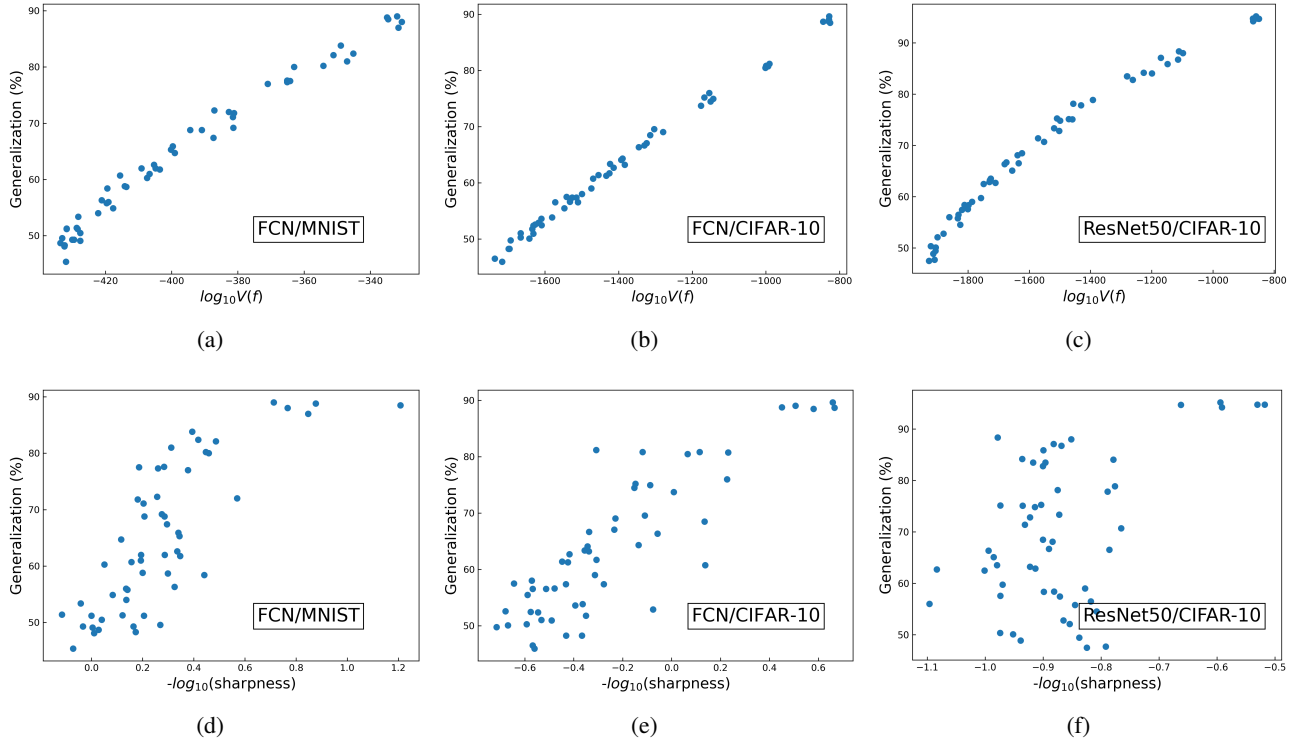


Figure 3. The correlation between volume $V(f)$, sharpness and generalization accuracy on MNIST and CIFAR-10. For MNIST $|S|=500$, $|E|=1000$; for CIFAR-10 $|S|=5000$, $|E|=2000$. The attack set size $|A|$ varies from 0 to $|S|$ and generates functions with different generalization performance. (a)-(c) depicts the correlation between generalization and volume for FCN on MNIST, FCN on CIFAR-10 and Resnet-50 on CIFAR-10, respectively. (d)-(f) show the correlation between generalization and sharpness for FCN on MNIST, FCN on CIFAR-10, and Resnet50 on CIFAR-10, respectively. In this experiment, all DNNs are trained with vanilla SGD.

from our arguments linking to the Bayesian posterior in section 3.

Figs.3(d)-(f) show that the correlation between sharpness and generalization is much more scattered than for volume. In appendix D we also show the direct correlation between volume and sharpness which closely resembles fig. 3(d)-(f) because $V(f)$ and ϵ correlate so tightly.

5.3. The effect of optimizer choice on flatness

To further support our hypothesis that volume is a much more robust predictor of generalization than flatness is, we test the effect of changing the optimizer from the vanilla SGD we used in fig. 3. We use Adam (Kingma & Ba, 2014), and entropy-SGD (Chaudhari et al., 2019) which includes an explicit term to maximise the flatness. Both SGD variants show good optimization performance for the standard default Tensorflow hyperparameters we use. In fact Adam is much more efficient than vanilla SGD, especially for CIFAR. Their generalization performance, however, does not significantly vary from plain SGD, and this is reflected in the volumes of the functions that they find. More impor-

tantly, fig. 4 shows that the generalization-flatness correlation can be broken by using these optimizers, whereas the volume-generalization correlation remains intact. A similar breakdown of the correlation persists upon overtraining and can also be seen for flatness measures that use Hessian eigenvalues (fig. S10 to fig. S15).

Changing optimizers or changing hyperparameters can, of course, alter the generalization performance by small amounts, which may be critically important in practical applications. Nevertheless, as demonstrated in Mingard et al. (2020), the overall effect of hyperparameter or optimizer changes is usually quite small on these scales. The large differences in sharpness/flatness generated simply by changing the optimizer suggests that flatness measures may not always reliably capture the effects of hyperparameter or optimizer changes. Note that we find less deterioration when comparing SGD to Adam for Resnet50 on CIFAR-10, (fig. S16). The exact nature of these effects remains subtle.

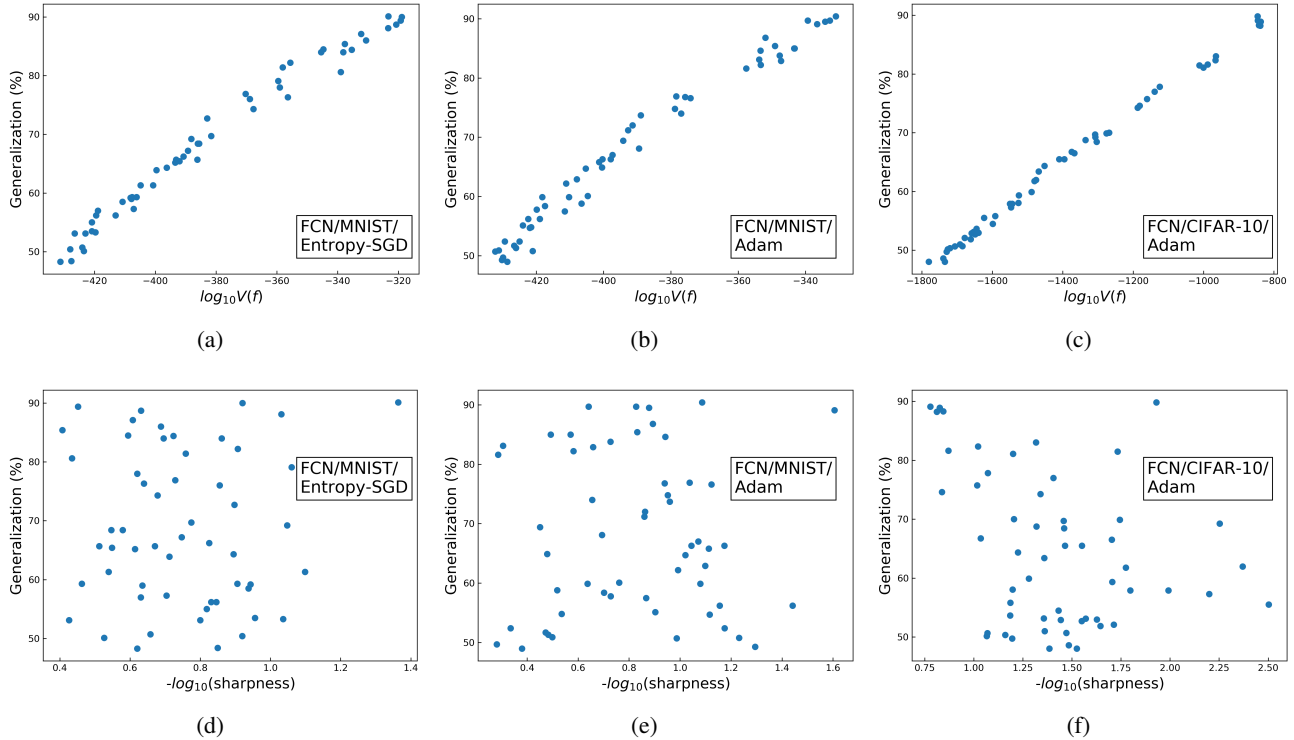


Figure 4. SGD-variants can break the flatness-generalization correlation, but not the volume-generalization correlation. The figures show generalization v.s. volume or sharpness for the FCN trained on (a) and (d) – MNIST with Entropy-SGD; (b) and (e) – MNIST with Adam; (c) and (f) – CIFAR-10 with Adam, for the same S and E as in fig. 3. Note that the correlation with the volume is virtually identical to vanilla SGD, but that the correlation with flatness changes significantly.

5.4. Temporal behavior of sharpness and volume

In the experiments above, the flatness and volume metrics are calculated at the epoch where the system first reaches 100% training accuracy. In fig. 5, we measure the volume and the sharpness for each epoch for our FCN, trained on MNIST (with no attack set). Zero training error is reached at epoch 140, and we overtrain for a further 1000 epochs. From initialization, both sharpness and volume reduce until zero-training error is reached. Subsequently, volume stays constant, but the cross-entropy loss continues to decrease, as expected for such classification problems. This leads to a reduction in sharpness, even though the function, its volume, and the training error don't change. This demonstrates that flatness is a relative concept that depends, for example, on the duration of training. In figs. S10 and S11 we show for an FCN on MNIST that the quality of flatness-generalization correlations are largely unaffected by overtraining, for both SGD and Adam respectively, even though the absolute values of the sharpness change substantially.

One of the strong critiques of flatness is that re-parameterisations such as the alpha-scaling transformation defined in eq. (1) can arbitrarily change local flatness mea-

asures (Dinh et al., 2017). Fig. 5 shows that alpha scaling indeed leads to a spike in the sharpness. As demonstrated in the inset, the volume is initially invariant upon alpha-scaling because $f(\mathbf{w})$ is unchanged. However, alpha-scaling can drive the system to unusual parts of the neutral space with steep gradients in the loss function, which mean that SGD falls off the zero training error manifold. Volume goes up because it is more likely to randomly fall onto large $V(f)$ functions. However, the system soon relaxes to essentially the same function and volume. In fig. S5, we show that it is possible to obtain a spike in sharpness without the volume ever changing, i.e. without leaving the neutral subspace. In each case, the sharpness rapidly decays after the spike, suggesting that alpha scaling brings the system into a parameter region that is "unnatural".

6. Discussion

The notion that flatness correlates with generalization is widely believed in the community, but the evidential basis for this hypothesis has always been mixed. Here we performed extensive empirical work showing that flatness can indeed correlate with generalization. However, this cor-

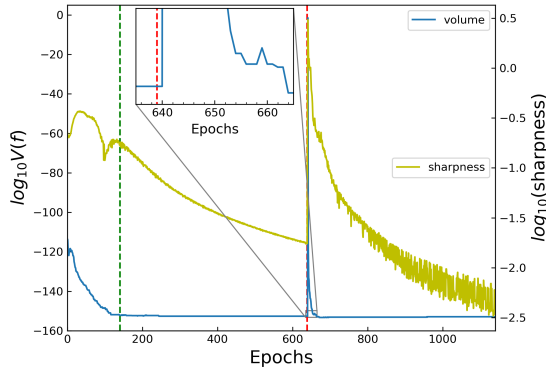


Figure 5. How sharpness and volume evolve with epochs. At each epoch we calculate the sharpness and the volume for our FCN on MNIST with $|S|=500$. The green dashed line denotes epoch 140 where zero-training error is reached and post-training starts. The red dashed line denotes epoch 639 where α -scaling takes place with $\alpha = 5.9$. Upon alpha-scaling, the sharpness increases markedly, but then quickly decreases again. The inset shows that the volume is initially unchanged after alpha-scaling. However, large gradients mean that in subsequent SGD steps, the function (and the volume) changes, before recovering to (nearly) the same function and volume.

relation is not always tight, and can be easily broken by alpha-scaling, or by changing the optimizer. By contrast, the volume, which is equivalent to the Bayesian prior $P(f)$ and directly proportional to the Bayesian posterior $P_B(f|S)$ for functions that give zero error on the training set, is a much more robust predictor of generalization.

While the generalization performance of a DNN can be successfully predicted by the marginal likelihood PAC-Bayes bound (Valle-Pérez et al., 2018; Valle-Pérez & Louis, 2020), no such tight bound exists (to our knowledge) linking generalization and the Bayesian prior or posterior of an individual function. Further theoretical work in this direction is needed.

Valle-Pérez et al. (2018) used an algorithmic information theory (AIT) inspired coding theorem (Dingle et al., 2018; 2020), and De Palma et al. (2018); Mingard et al. (2019) used direct analytic approaches to argue that DNNs are intrinsically biased towards functions with low Kolmogorov complexity $K(f)$. This *simplicity bias* means that high $P(f)$ functions have low $K(f)$, and high $K(f)$ functions have low $P(f)$. Since it is widely thought that data such as MNIST and CIFAR-10 are simple (Lin et al., 2017; Goldt et al., 2019; Spigler et al., 2019), an inbuilt inductive bias towards low $K(f)$ functions, which is a kind of built in *Occam’s razor*, should help facilitate good generalization, as is indeed observed for DNNs. The AIT arguments above further suggest a general scaling of the form: $-\log(V(f)) \propto K(f)$.

A simple reason flatness measures correlate with generalization is because they correlate with volume. There may be independent arguments for why flatness correlates with generalization, even if only imperfectly. Sketches in the literature (Hinton & van Camp, 1993; Schmidhuber, 1997) based for example on MDL (Rissanen, 1978) or linking flatness to smoothness of functions (Wu et al., 2017) suggest potential deep links to the AIT arguments for simplicity bias in DNNs (Valle-Pérez et al., 2018).

There is a rich literature deriving generalization bounds based on concepts related to flatness in parameter space, see e.g. Jiang et al. (2019); Dziugaite et al. (2020); Valle-Pérez & Louis (2020) for recent reviews of this voluminous literature. Links between local volume and generalization have been explored in the context of bounds, at least since Shawe-Taylor & Williamson (1997), if not earlier.

Flatness measures are parameter dependent, whereas we approximate our volumes, which correlate better with generalization, using the the non-parametric GP approximation. Valle-Pérez & Louis (2020) showed that the function based marginal-likelihood PAC-Bayes bound should always be tighter than parameter based versions of the same PAC-Bayes bound, again suggesting that parameter based approaches may not be the best avenue for deriving predictors of generalization.

The fact that volume, which is calculated without reference to SGD, works so well as a predictor for the generalization error of SGD trained DNNs strongly suggests that any extra inductive bias of SGD, beyond that already present in the parameter-function map, is small on these scales. SGD is indeed biased towards flat minima, but primarily because these have a larger volume. These results are consistent with those of Mingard et al. (2020) who showed that the probability that SGD converges on a particular function f is predicted by the posterior $P_B(f|S) \propto P(f)$.

Future work includes linking flatness and volume to concepts which correlate with generalization such as frequency (Rahaman et al., 2018; Xu et al., 2019), or the sensitivity to changes in the inputs (Arpit et al., 2017; Novak et al., 2018a). Improvements to the GP approximations we make are an important technical goal. Volume can be expensive to calculate, so finding reliable local approximations related to flatness may still be a worthy endeavour. Finally, our main result –that volume, or the prior upon initialization, correlates so well with generalization – still requires a proper theoretical underpinning. Such explanations will need to include not just the networks and the algorithms, but also the data (Zdeborová, 2020).

References

- Arpit, D., Jastrzebski, S., Ballas, N., Krueger, D., Bengio, E., Kanwal, M. S., Maharaj, T., Fischer, A., Courville, A., Bengio, Y., et al. A closer look at memorization in deep networks. *arXiv preprint arXiv:1706.05394*, 2017.
- Byrd, R. H., Lu, P., Nocedal, J., and Zhu, C. A limited memory algorithm for bound constrained optimization. *SIAM Journal on scientific computing*, 16(5):1190–1208, 1995.
- Chaudhari, P., Choromanska, A., Soatto, S., LeCun, Y., Baldassi, C., Borgs, C., Chayes, J., Sagun, L., and Zecchina, R. Entropy-sgd: Biasing gradient descent into wide valleys. *Journal of Statistical Mechanics: Theory and Experiment*, 2019(12):124018, 2019.
- Cho, Y. and Saul, L. Kernel methods for deep learning. *Advances in neural information processing systems*, 22: 342–350, 2009.
- De Palma, G., Kiani, B. T., and Lloyd, S. Random deep neural networks are biased towards simple functions. *arXiv preprint arXiv:1812.10156*, 2018.
- Dingle, K., Camargo, C. Q., and Louis, A. A. Input–output maps are strongly biased towards simple outputs. *Nature Communications*, 9(1):1–7, 2018.
- Dingle, K., Pérez, G. V., and Louis, A. A. Generic predictions of output probability based on complexities of inputs and outputs. *Scientific Reports*, 10(1):1–9, 2020.
- Dinh, L., Pascanu, R., Bengio, S., and Bengio, Y. Sharp minima can generalize for deep nets. In *Proceedings of the 34th International Conference on Machine Learning—Volume 70*, pp. 1019–1028. JMLR. org, 2017.
- Duchi, J., Hazan, E., and Singer, Y. Adaptive subgradient methods for online learning and stochastic optimization. *Journal of machine learning research*, 12(Jul):2121–2159, 2011.
- Dziugaite, G. K., Drouin, A., Neal, B., Rajkumar, N., Caballero, E., Wang, L., Mitliagkas, I., and Roy, D. M. In search of robust measures of generalization. *arXiv preprint arXiv:2010.11924*, 2020.
- Goldt, S., Mézard, M., Krzakala, F., and Zdeborová, L. Modelling the influence of data structure on learning in neural networks. *arXiv preprint arXiv:1909.11500*, 2019.
- Goyal, P., Dollár, P., Girshick, R., Noordhuis, P., Wesolowski, L., Kyrola, A., Tulloch, A., Jia, Y., and He, K. Accurate, large minibatch sgd: Training imagenet in 1 hour. *arXiv preprint arXiv:1706.02677*, 2017.
- He, K., Zhang, X., Ren, S., and Sun, J. Deep residual learning for image recognition. In *Proceedings of the IEEE conference on computer vision and pattern recognition*, pp. 770–778, 2016.
- Hinton, G. E. and van Camp, D. Keeping neural networks simple. In *International Conference on Artificial Neural Networks*, pp. 11–18. Springer, 1993.
- Hochreiter, S. and Schmidhuber, J. Flat minima. *Neural Computation*, 9(1):1–42, 1997.
- Hoffer, E., Hubara, I., and Soudry, D. Train longer, generalize better: closing the generalization gap in large batch training of neural networks. In *Advances in neural information processing systems*, pp. 1731–1741, 2017.
- Ioffe, S. and Szegedy, C. Batch normalization: Accelerating deep network training by reducing internal covariate shift. *arXiv preprint arXiv:1502.03167*, 2015.
- Izmailov, P., Podoprikin, D., Garipov, T., Vetrov, D., and Wilson, A. G. Averaging weights leads to wider optima and better generalization. *arXiv preprint arXiv:1803.05407*, 2018.
- Jastrzebski, S., Kenton, Z., Arpit, D., Ballas, N., Fischer, A., Bengio, Y., and Storkey, A. J. Finding flatter minima with sgd. In *ICLR (Workshop)*, 2018.
- Jiang, Y., Neyshabur, B., Mobahi, H., Krishnan, D., and Bengio, S. Fantastic generalization measures and where to find them. *arXiv preprint arXiv:1912.02178*, 2019.
- Keskar, N. S., Mudigere, D., Nocedal, J., Smelyanskiy, M., and Tang, P. T. P. On large-batch training for deep learning: Generalization gap and sharp minima. *arXiv preprint arXiv:1609.04836*, 2016.
- Kingma, D. P. and Ba, J. Adam: A method for stochastic optimization. *arXiv preprint arXiv:1412.6980*, 2014.
- Krizhevsky, A., Hinton, G., et al. Learning multiple layers of features from tiny images. 2009.
- LeCun, Y., Bottou, L., Bengio, Y., and Haffner, P. Gradient-based learning applied to document recognition. *Proceedings of the IEEE*, 86(11):2278–2324, 1998.
- Lee, J., Bahri, Y., Novak, R., Schoenholz, S. S., Pennington, J., and Sohl-Dickstein, J. Deep neural networks as gaussian processes. *arXiv preprint arXiv:1711.00165*, 2017.
- Lin, H. W., Tegmark, M., and Rolnick, D. Why does deep and cheap learning work so well? *Journal of Statistical Physics*, 168(6):1223–1247, 2017.

- Maddox, W. J., Benton, G., and Wilson, A. G. Rethinking parameter counting in deep models: Effective dimensionality revisited. *arXiv preprint arXiv:2003.02139*, 2020.
- Manrubia, S., Cuesta, J. A., Aguirre, J., Ahnert, S. E., Altenberg, L., Cano, A. V., Catalán, P., Diaz-Uriarte, R., Elena, S. F., García-Martín, J. A., et al. From genotypes to organisms: State-of-the-art and perspectives of a cornerstone in evolutionary dynamics. *arXiv preprint arXiv:2002.00363*, 2020.
- Matthews, A. G. d. G., Rowland, M., Hron, J., Turner, R. E., and Ghahramani, Z. Gaussian process behaviour in wide deep neural networks. *arXiv preprint arXiv:1804.11271*, 2018.
- McAllester, D. A. Some pac-bayesian theorems. In *Proceedings of the eleventh annual conference on Computational learning theory*, pp. 230–234. ACM, 1998.
- Mingard, C., Skalse, J., Valle-Pérez, G., Martínez-Rubio, D., Mikulik, V., and Louis, A. A. Neural networks are a priori biased towards boolean functions with low entropy. *arXiv preprint arXiv:1909.11522*, 2019.
- Mingard, C., Valle-Pérez, G., Skalse, J., and Louis, A. A. Is sgd a bayesian sampler? well, almost. *arXiv preprint arXiv:2006.15191*, 2020.
- Neal, R. M. Priors for infinite networks (tech. rep. no. crg-tr-94-1). *University of Toronto*, 1994.
- Novak, R., Bahri, Y., Abolafia, D. A., Pennington, J., and Sohl-Dickstein, J. Sensitivity and generalization in neural networks: an empirical study. *arXiv preprint arXiv:1802.08760*, 2018a.
- Novak, R., Xiao, L., Lee, J., Bahri, Y., Yang, G., Hron, J., Abolafia, D. A., Pennington, J., and Sohl-Dickstein, J. Bayesian deep convolutional networks with many channels are gaussian processes. *arXiv preprint arXiv:1810.05148*, 2018b.
- Petzka, H., Adilova, L., Kamp, M., and Sminchisescu, C. A reparameterization-invariant flatness measure for deep neural networks. *arXiv preprint arXiv:1912.00058*, 2019.
- Rahaman, N., Baratin, A., Arpit, D., Draxler, F., Lin, M., Hamprecht, F. A., Bengio, Y., and Courville, A. On the spectral bias of neural networks. *arXiv preprint arXiv:1806.08734*, 2018.
- Rangamani, A., Nguyen, N. H., Kumar, A., Phan, D., Chin, S. H., and Tran, T. D. A scale invariant flatness measure for deep network minima. *arXiv preprint arXiv:1902.02434*, 2019.
- Rasmussen, C. E. Gaussian processes in machine learning. In *Summer School on Machine Learning*, pp. 63–71. Springer, 2003.
- Rissanen, J. Modeling by shortest data description. *Automatica*, 14(5):465–471, 1978.
- Rumelhart, D. E., Hinton, G. E., and Williams, R. J. Learning representations by back-propagating errors. *Nature*, 323(6088):533–536, 1986.
- Sagun, L., Bottou, L., and LeCun, Y. Eigenvalues of the hessian in deep learning: Singularity and beyond. *arXiv preprint arXiv:1611.07476*, 2016.
- Schaper, S. and Louis, A. A. The arrival of the frequent: how bias in genotype-phenotype maps can steer populations to local optima. *PloS one*, 9(2):e86635, 2014.
- Schmidhuber, J. Discovering neural nets with low kolmogorov complexity and high generalization capability. *Neural Networks*, 10(5):857–873, 1997.
- Shawe-Taylor, J. and Williamson, R. C. A pac analysis of a bayesian estimator. In *Annual Workshop on Computational Learning Theory: Proceedings of the tenth annual conference on Computational learning theory*, volume 6, pp. 2–9, 1997.
- Smith, S. L., Kindermans, P.-J., Ying, C., and Le, Q. V. Don’t decay the learning rate, increase the batch size. *arXiv preprint arXiv:1711.00489*, 2017.
- Spigler, S., Geiger, M., and Wyart, M. Asymptotic learning curves of kernel methods: empirical data vs teacher-student paradigm. *arXiv preprint arXiv:1905.10843*, 2019.
- Tan, M. Expectation propagation of gaussian process classification and its application to gene expression analysis. 01 2008.
- Tieleman, T. and Hinton, G. Lecture 6.5-rmsprop: Divide the gradient by a running average of its recent magnitude. *COURSERA: Neural networks for machine learning*, 4(2):26–31, 2012.
- Tsuzuku, Y., Sato, I., and Sugiyama, M. Normalized flat minima: Exploring scale invariant definition of flat minima for neural networks using pac-bayesian analysis. *arXiv preprint arXiv:1901.04653*, 2019.
- Valle-Pérez, G. and Louis, A. A. Generalization bounds for deep learning. *arXiv preprint arXiv:2012.04115*, 2020.
- Valle-Pérez, G., Camargo, C. Q., and Louis, A. A. Deep learning generalizes because the parameter-function map is biased towards simple functions. *arXiv preprint arXiv:1805.08522*, 2018.

- Wei, M. and Schwab, D. J. How noise affects the hessian spectrum in overparameterized neural networks. *arXiv preprint arXiv:1910.00195*, 2019.
- Wu, L., Zhu, Z., et al. Towards understanding generalization of deep learning: Perspective of loss landscapes. *arXiv preprint arXiv:1706.10239*, 2017.
- Xu, Z.-Q. J., Zhang, Y., Luo, T., Xiao, Y., and Ma, Z. Frequency principle: Fourier analysis sheds light on deep neural networks. *arXiv preprint arXiv:1901.06523*, 2019.
- Yao, Z., Gholami, A., Lei, Q., Keutzer, K., and Mahoney, M. W. Hessian-based analysis of large batch training and robustness to adversaries. In *Advances in Neural Information Processing Systems*, pp. 4949–4959, 2018.
- Zdeborová, L. Understanding deep learning is also a job for physicists. *Nature Physics*, 16(6):602–604, 2020.
- Zhang, Y., Saxe, A. M., Advani, M. S., and Lee, A. A. Energy–entropy competition and the effectiveness of stochastic gradient descent in machine learning. *Molecular Physics*, 116(21-22):3214–3223, 2018.

A. Gaussian process approximation of the volume

In this section, we sketch out how we calculated the volume of a function $V(f)$, which is equivalent to earlier calculations of the Bayesian prior over functions $P(f)$ (Valle-Pérez et al., 2018; Mingard et al., 2020). As in those papers, we use Gaussian processes, which have been shown to be equivalent to DNNs in the limit of infinite layer width (Neal, 1994; Lee et al., 2017; Matthews et al., 2018; Tan, 2008; Rasmussen, 2003). These neural network GPs (NNGPs) have been shown to accurately approximate the prior over functions $P(f)$ of finite-width Bayesian DNNs (Valle-Pérez et al., 2018; Matthews et al., 2018; Mingard et al., 2020).

For the NNGPs, a GP prior is placed on the pre-activations \mathbf{z} of the last layer of the neural network (before a final non-linearity, e.g. softmax, is applied), meaning that for any finite inputs set $\mathbf{x} = \{x_1, \dots, x_m\}$, the random output vector (pre-activations) $\mathbf{z} = [z(x_1), \dots, z(x_m)]^T$ has a Gaussian distribution. Note that in this paper, the the last layer has a single activation since we only focus on binary classification. Without loss of generality, we can assume such a process has a zero mean. The prior probability of the outputs \mathbf{z} can be calculated as:

$$P(\mathbf{z}) = \frac{1}{(2\pi)^{\frac{m}{2}} \Sigma^{\frac{1}{2}}} \exp\left(-\frac{1}{2} \mathbf{z}^T \Sigma^{-1} \mathbf{z}\right) \quad (5)$$

Σ is the covariance matrix (often called kernel), whose entries are defined as $\Sigma(x_i, x_j) \equiv \mathbb{E}[z(x_i), z(x_j)]$. Neal (1994) gave the basic form of kernel Σ in single hidden layer case, where Σ depends on the variance of weights and biases (σ_w and σ_b). In DNNs with multiple hidden layers, the kernel for layer l can be calculated recursively by induction, assuming the layer $l-1$ is a GP (Lee et al., 2017; Matthews et al., 2018). The kernel for fully connected ReLU-activated networks has a well known *arc-cosine kernel* analytical form (Cho & Saul, 2009), which we used in all FCNs in our work.

For ResNet50, the analytical form of GP kernel is intractable. Instead, we use a Monte Carlo empirical kernel (Novak et al., 2018b), and apply one step of the fully connected GP recurrence relation (Lee et al., 2017), taking advantage of the fact that the last layer of ResNet50 is fully connected. Mathematically, the empirical kernel can be expressed as:

$$\tilde{\Sigma}(x_i, x_j) := \frac{\sigma_w^2}{Mn} \sum_{m=1}^M \sum_{c=1}^n (h_{\mathbf{w}_m}^{L-1}(x_i))_c (h_{\mathbf{w}_m}^{L-1}(x_j))_c + \sigma_b^2 \quad (6)$$

where $(h_{\mathbf{w}_m}^{L-1}(x))_c$ is the activation of c -th neuron in the last hidden layer (L is the total number of layers) for the network parameterized by the m -th sampling of parameters \mathbf{w}_m , M is the number of total Monte Carlo sampling, n is the width of the final hidden layer, and σ_w, σ_b are the weights and biases variance respectively. In our experiments, M is set to be $0.1 \times (|S| + |E|)$.

After calculating $P(\mathbf{z})$ with the corresponding kernel, the prior P over (coarse-grained) functions $P(f)$ can be calculated through likelihood $P(f|\mathbf{z})$, which in our case is just a Heaviside function representing a hard sign nonlinearity. As this likelihood produces an intractable $P(f)$, we used Expectation Propagation (EP) algorithm for the approximation of $P(f)$ (Rasmussen, 2003). This same EP approximation was used in Mingard et al. (2020) where it is discussed further. We represent the function f by the input-output pairs on the concatenation of training set and test set ($S + E$).

B. Comparing flatness metrics

As mentioned in section 2.2 of the main text, the sharpness metric in definition 2.1 can be directly linked to spectral norm of the Hessian by considering the second order Taylor expansion of $L(\mathbf{w})$ around a critical point in powers of ϵ (Dinh et al., 2017). We empirically confirm this relationship by showing in fig. S1 the direct correlation between sharpness and spectral norm of Hessian, as well as in fig. S2 the correlation between Hessian spectral norm and volume in Boolean system described in section 5.1.

In addition to the spectral norm, another widely used flatness measure is the product of a subset of the positive Hessian eigenvalues, typically say the product of the top-50 largest eigenvalues (Wu et al., 2017; Zhang et al., 2018). We measured the correlation of these Hessian-based flatness metrics with sharpness as well as with generalization for the FCN/MNIST system in fig. S3. Since they correlate well with the sharpness, these flatness measures show very similar correlations with generalization as sharpness does in fig. 3 and fig. 4. In other words, the Hessian-based flatness metrics also capture the loose correlation with generalization when the neural network is trained by SGD and the deterioration of this correlation when we change the optimizer to Adam.

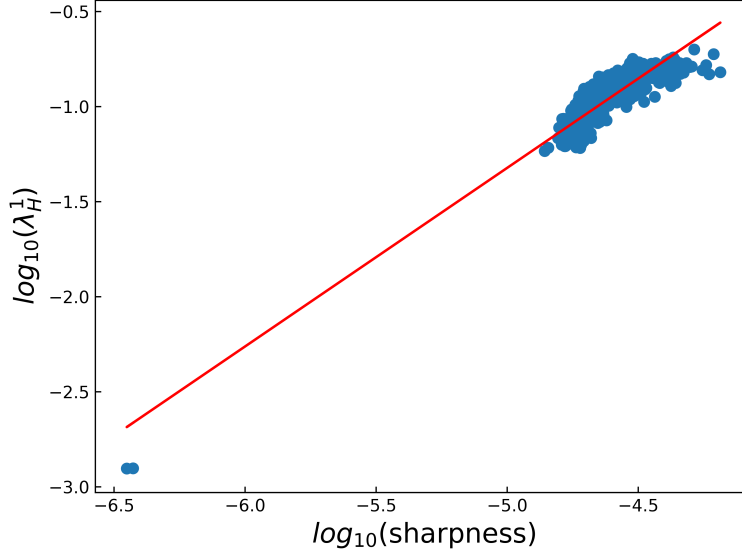


Figure S1. The direct correlation between sharpness and spectral norm of Hessian for the 1000 most frequently found functions found after SGD runs for a two hidden layer FCN, in the $n = 7$ Boolean system (Same system as in fig. 2) .

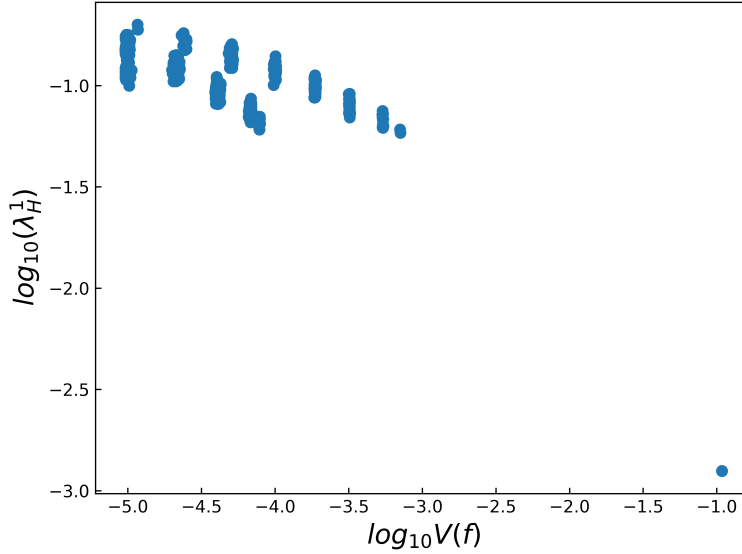


Figure S2. The correlation between volume and flatness in Boolean system where the flatness is measured by spectral norm of Hessian, for the 1000 most frequently occurring functions found by SGD runs with a two hidden layer FCN. The system is the same $n = 7$ Boolean system as in fig. 2 except that we use a different metric of flatness.

Another detail worth noting is that [Keskar et al. \(2016\)](#) used the L-BFGS-B algorithm ([Byrd et al., 1995](#)) to perform the maximization of $L(\mathbf{w})$ in \mathcal{C}_ϵ , which is the box boundary around the minimum of interest:

$$\mathcal{C}_\epsilon = \{\Delta \mathbf{w} \in \mathbb{R}^n : -\epsilon(|w_i| + 1) \leq \Delta w_i \leq \epsilon(|w_i| + 1) \quad \forall i \in \{1, 2, \dots, n\}\} \quad (7)$$

However, as a quasi-Newton method, L-BFGS-B is not scalable when there are tens of millions of parameters in modern DNNs. To make Keskar-sharpness applicable for large DNNs (e.g. ResNet50), we use vanilla SGD for the maximization instead. The hyperparameters for the sharpness calculation are listed in table 1. Note that the entries batch size, learning rate and number of epochs all refer to the SGD optimizer which does the maximization in the sharpness calculation process.

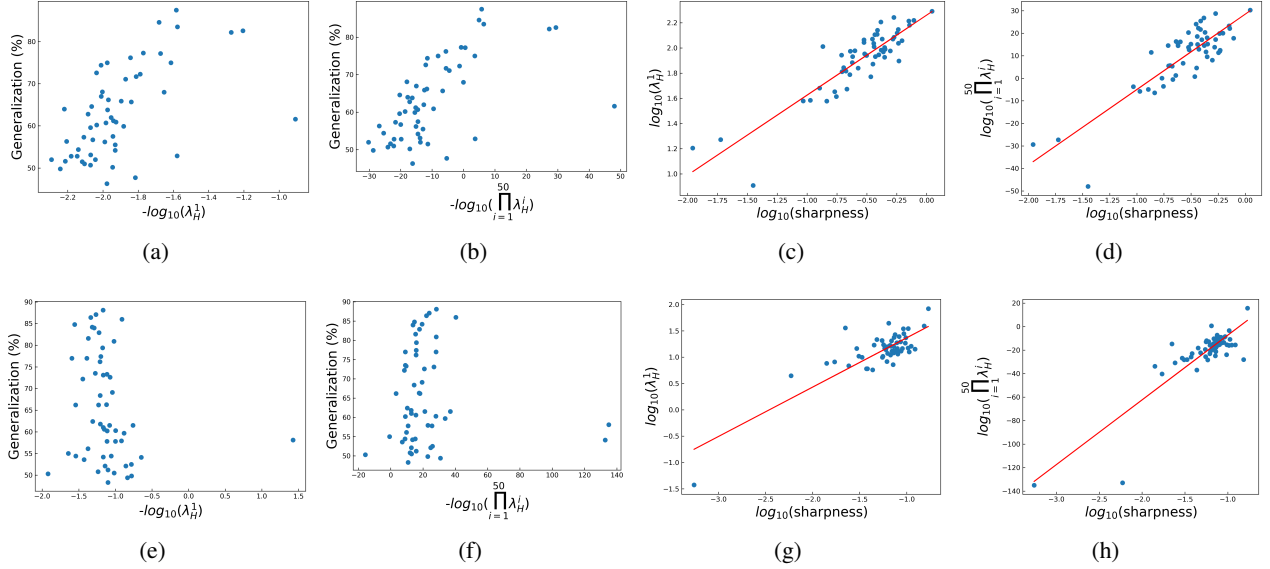


Figure S3. Two Hessian-based flatness metrics show analogous behavior to sharpness defined in (definition 2.1). The architecture and dataset are FCN/MNIST, with training set size $|S| = 500$, and test set size $|E| = 1000$; which are the same settings as fig. 3 (d) and fig. 4 (e). **Optimizer: SGD** (a) - (b): The correlation between Hessian-based flatness metrics and generalization. (c) - (d): Sharpness and Hessian-based flatness metrics correlate well with one another. **Optimizer: Adam** (e) - (f): The correlation between Hessian-based flatness metrics and generalization breaks down, just as it does for sharpness in fig. 4. (g) - (h): Sharpness and Hessian-based flatness metrics correlate well with one another, even though they don't correlate well with generalization.

Table 1. Hyperparameters for sharpness calculation

DATA SET	ARCHITECTURE	BOX SIZE (ϵ)	BATCH SIZE	LEARNING RATE	NUMBER OF EPOCHS
BOOLEAN	FCN	10^{-4}	16	10^{-3}	10
MNIST	FCN	10^{-4}	32	10^{-3}	100
CIFAR10	FCN	10^{-5}	128	5×10^{-5}	100
CIFAR10	RESNET50	10^{-5}	128	10^0	100

The number of epochs is chosen such that the max value of loss function found at each maximization step converges. An example of the convergence of sharpness is shown in fig. S4. As a check, we also compared our SGD-sharpness with the original L-BFGS-B-sharpness, finding similar results.

C. Implementing alpha scaling

In this section we describe in detail how we implement the alpha scaling in DNNs first proposed by Dinh et al. (2017). The widely used rectified linear activation (ReLU) function

$$\phi_{\text{rect}}(x) = \max(x, 0)$$

exhibits the so-called “non-negative homogeneity” property:

$$\forall(z, \alpha) \in \mathbb{R} \times \mathbb{R}^+, \phi_{\text{rect}}(z\alpha) = \alpha\phi_{\text{rect}}(z)$$

The action of a L -layered deep feed-forward neural network can be written as:

$$y = \phi_{\text{rect}}(\phi_{\text{rect}}(\dots \phi_{\text{rect}}(x \cdot W_1 + b_1) \dots) \cdot W_{L-1} + b_{L-1}) \cdot W_L + b_L$$

in which

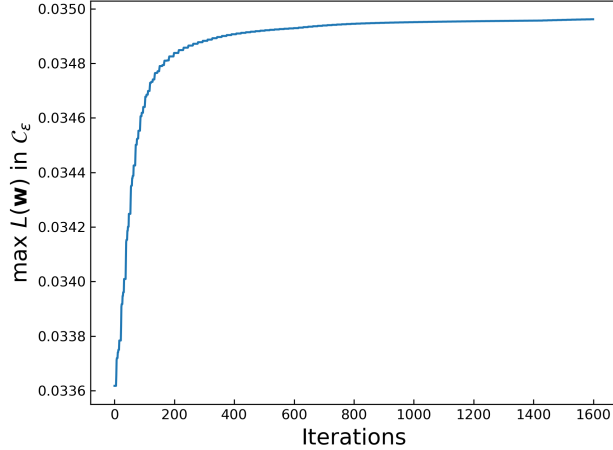


Figure S4. The max value of loss function $L(\mathbf{w})$ at each iteration in the process of maximization, when calculating the sharpness using SGD instead of L-BFGS-B. The plot shows the max loss value found by SGD in the box limit C_ϵ will converge after given number of epochs. For this plot the hyperparameters are listed in the second line of table 1 (MNIST).

- x is the input vector
- W_L is the weight matrix of the L -th layer
- b_L is the bias vector of the L -th layer

To simplify notation, we have not included the final activation function, which may take any form (softmax or sigmoid etc.) without modification of the proceeding arguments. Generalizing the original arguments from Dinh et al. (2017) slightly to include bias terms, we exploit the non-negative homogeneity of the ReLU function to find that a so-called “ α -scaling” of one of the layers will not change its behaviour. Explicitly applying this to the i -th layer yields:

$$(\phi_{\text{rect}}(x \cdot \alpha W_i + \alpha b_i)) \cdot \frac{1}{\alpha} W_{i+1} = (\phi_{\text{rect}}(x \cdot W_i + b_i)) \cdot W_{i+1} \quad (8)$$

Clearly, the transformation described by $(W_i, b_i, W_{i+1}) \rightarrow (\alpha W_i, \alpha b_i, \frac{1}{\alpha} W_{i+1})$ will lead to an observationally equivalent network (that is, a network whose output is identical for any given input, even if the weight and bias terms differ).

Since the α scaling transformation does not change the function, it does not change the volume of the function. However, for large enough α , as shown for example in fig. 5, we see that SGD can be “knocked” out of the current neutral space because of the large gradients that are induced by the α scaling. This typically leads to the volume suddenly surging up, because the random nature of the perturbation means that the system is more likely to land on large volume functions. However, we always observe that the volume then drops back down quite quickly as SGD reaches zero training error again. On the other hand, as shown in fig. S5, when the value of α is smaller it does not knock SGD out of the neutral space, and so the volume does not change at all. Nevertheless, the sharpness still exhibits a strong spike due to the the alpha scaling.

Although not in the scope of this work, it is worth noting that the alpha scaling process in Convolutional Neural Networks (CNNs) with batch normalization (Ioffe & Szegedy, 2015) layer(s) is somewhat different. Because a batch normalization layer will eliminate all affine transformations applied on its inputs, one can arbitrarily alpha scale the layers before a batch normalization layer without needing to of compensate in following layer, provided the scaling is linear.

D. Flatness and volume correlation

In the main text, we showed the correlation of volume and of sharpness with generalization in fig. 3 and fig. 4. Here, in fig. S6, we show the direct correlation of volume and sharpness. As expected from the figures in the main text, sharpness correlates with volume roughly as it does with generalization - i.e. reasonably for vanilla SGD but badly for entropy-SGD (Chaudhari et al., 2019) or Adam (Kingma & Ba, 2014). We note that, as shown in fig. S3, sharpness also correlates relatively well with

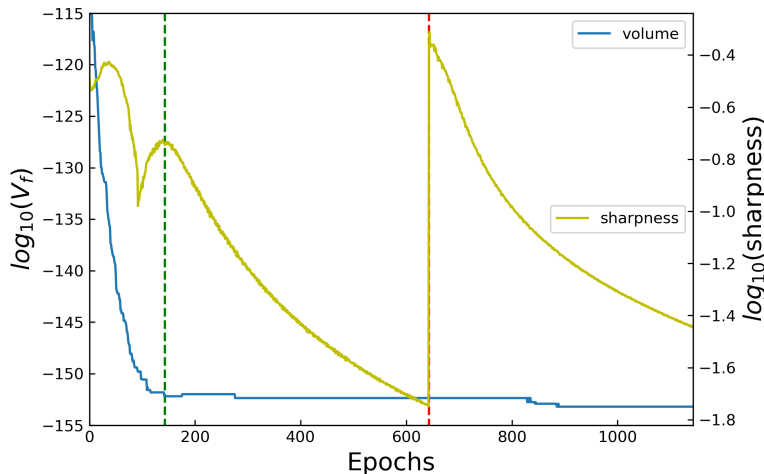


Figure S5. The effect of alpha scaling on volume and sharpness. At each epoch we calculate the sharpness and the volume for our FCN on MNIST system with $|S| = 500$. The green dashed line denotes where zero-training error is reached and post-training starts. The red dashed line denotes the epoch where α -scaling takes place with $\alpha = 5.0$. Here the value of α is not big enough to “knock” the optimizer out of the neutral space, in contrast to fig. 5. As expected, we observe no change in volume upon alpha scaling (note that volume can change on overtraining if a slightly different function is found by SGD). The sharpness shows a larger peak upon alpha-scaling, as expected. See appendix E.

the Frobenius norm of the Hessian and log product of its 50 largest eigenvalues for all the optimizers. So the correlation of flatness with volume/generalization does not depend much on which particular flatness measure is used.

Overall, it is perhaps unsurprising that a local measure such as flatness varies in how well it approximates the global volume. What is unexpected (at least to us) is that Adam and Entropy-SGD break the correlation for this data set. In appendix G.2, we show that this correlation also breaks down for other more complex optimizers, but, interestingly, not for full-batch SGD. Further empirical and theoretical work is needed to understand this phenomenon. For example, is the optimizer dependence of the correlation between flatness and volume a general property of the optimizer, or is it specific to certain architectures and datasets? One hint that these results may have complex dependencies on architecture and dataset comes from our observation that for ResNet50 on Cifar10, we see less difference between SGD and Adam than we see for the FCN on MNIST. More work is needed here.

E. Temporal behavior of sharpness

When using sharpness in definition 2.1 as the metric of flatness, there are several caveats. First is the hyperparameters (see table 1): the value of sharpness is only meaningful under specified hyperparameters, and in different experiments the sharpnesses are only comparable when the hyperparameters are the same. This renders sharpness less convenient to use (but still much more efficient than Hessian calculation). Second is the time evolving behavior of sharpness: For the classification problems we study, and for cross-entropy loss, it can continue to change even when the function (and hence generalization) is unchanged.

Before reaching zero training error, gradients can be large, and the behavior of sharpness (definition 2.1) can be unstable under changes of box size ϵ . This effect is likely the cause of some unusual fluctuations in the sharpness that can be observed in fig. 5 and fig. S5 around epoch 100. In fig. S7 we show that this artefact disappears for larger ϵ . Similarly, when the gradients are big (typical in training), sharpness may no longer link to spectral norm of Hessian very well.

In fig. S8, we first train the FCN to zero error, then “alpha scale” after 500 epochs, and then keep post-training for another 5000 epochs, much longer than in fig. 5. The behaviour of sharpness and volume upon “alpha scaling” (not surprisingly) follows our discussion in section 5.4. What is interesting to see here is that after enough overtraining, the effect of the alpha scaling spike appears to disappear, and the overall curve looks like a continuation of the curve prior to alpha scaling. What

WHY FLATNESS CORRELATES WITH GENERALIZATION FOR DEEP NEURAL NETWORKS

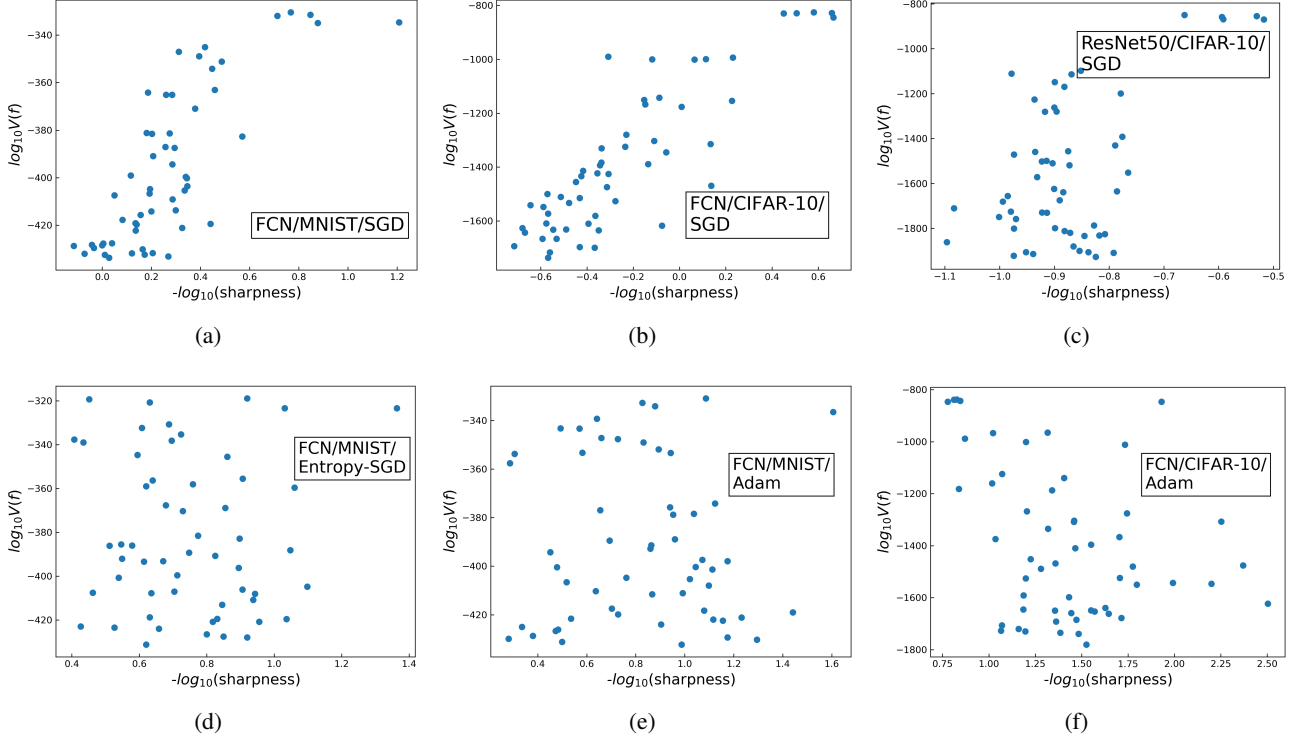


Figure S6. The direct correlation between volume $V(f)$ and sharpness over different datasets and optimizers. The correlation between volume and sharpness closely resembles the correlation between sharpness and generalization, mainly because volume and generalization are very closely correlated, as seen in our experiments (fig. 3, fig. 4).

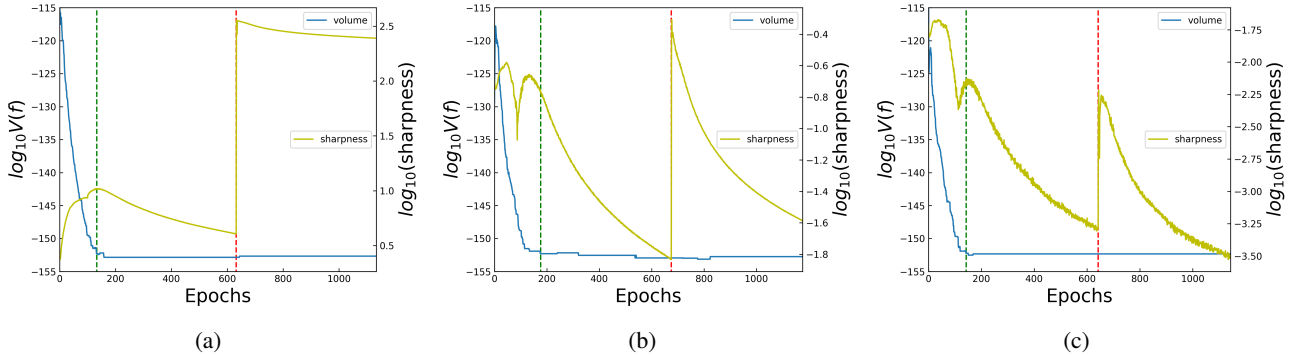


Figure S7. Different temporal behavior of sharpness, volume and accuracy when using different box size ϵ . The dataset is MNIST with $|S| = 500$ and $|E| = 100$. The architecture is FCN. SGD optimizer is used. Scaling parameter $\alpha = 5.0$. Green and red dashed line denote reaching zero training error and alpha scaling, respectively. (a) $\epsilon = 10^{-3}$, (b) $\epsilon = 10^{-4}$, (c) $\epsilon = 10^{-5}$. While there are quantitative differences between the values of ϵ used, qualitatively we observe similar behaviour.

this suggests is that alpha-scaling brings the system to an area of parameter space that is somehow “unnatural”. Again, this is a topic that deserves further investigation in the future.

Finally, we show the temporal behavior of a Hessian-based flatness measure in fig. S9. Because of the large memory cost when calculating the Hessian, we use a smaller FCN on MNIST, with the first hidden layer having 10 units. We find that the Hessian based flatness exhibit similar temporal behavior to sharpness.

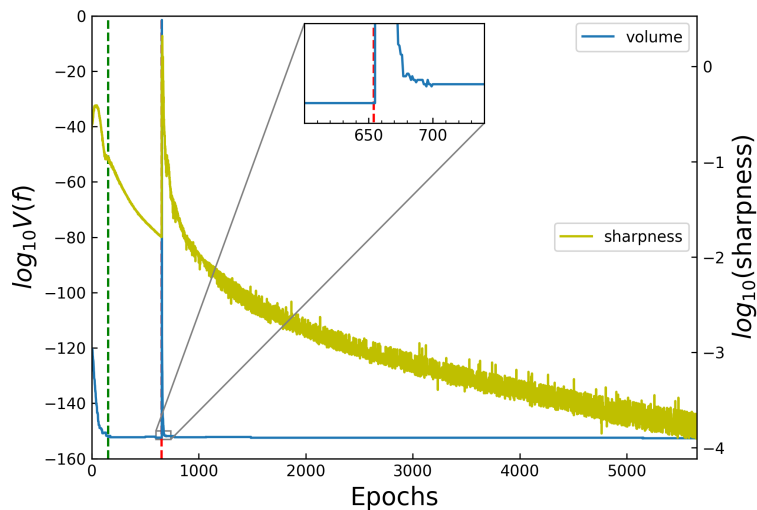


Figure S8. The temporal behavior of sharpness and volume after 5000 epochs of reaching zero training error. The dataset is MNIST with $|S| = 500$ and $|E| = 100$. The architecture is FCN. SGD optimizer is used. The magnitude of scaling $\alpha = 6.0$.

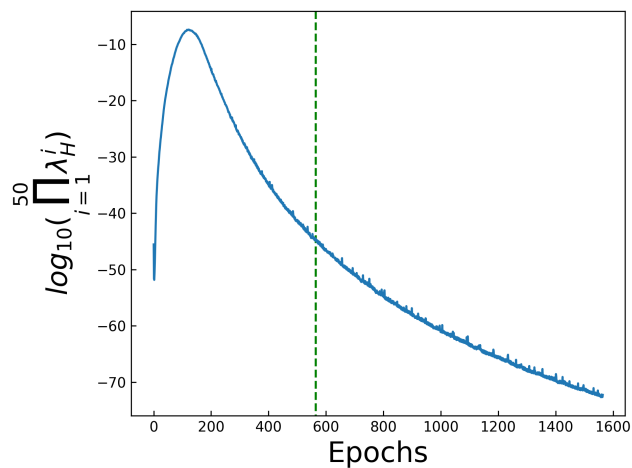


Figure S9. The temporal behavior of one Hessian based flatness metric. The dataset is MNIST with $|S| = 500$ and $|E| = 100$. The architecture is a smaller FCN (784-10-40-1), the optimizer is SGD. The green dashed line denotes the epoch where the system reaches zero training error. No alpha scaling is applied here. The Hessian based flatness metric shows similar temporal behaviour to the sharpness measure.

F. The correlation between generalization, volume, and sharpness upon overtraining

As shown in fig. 5 of the main text, and further discussed in appendix E, flatness measures keep decreasing upon overtraining even when the function itself does not change. In this section, we revisit the correlation between volume, flatness and generalization at different numbers of overtraining epochs, i.e. *after* reaching zero training error. As can be seen in fig. S10 to fig. S15, overtraining does not meaningfully affect the correlation between sharpness, volume, and generalization we observed at the epoch where zero error is first reached in fig. 3 and fig. 4. When the optimizer is SGD, the flatness, no matter if it is measured by sharpness or Hessian based metrics, correlates well with volume and (hence) generalization across different overtraining epochs; whereas when using Adam, the poor correlation also persists in overtraining.

G. Further experiments

G.1. ResNet50 trained with Adam

When training ResNet50 on CIFAR-10, we use training set size $|S| = 5000$, attack set size $|A| = 5000$, test set size $|E| = 2000$. In each experiment, we mix the whole training set with different size of subset of attack set. The size of $|A|$ ranges as $(0, 500, 1000, 1500, \dots, 5000)$. For each subset of attack set we sample 5 times. When training ResNet50 with Adam, we empirically found it is hard to train the neural net to zero training error with attack set size $|A| > 2500$. So we only show the results for those functions found with $|A| \leq 2500$. In fig. S16 we show the results of correlation between sharpness and volume with generalization with limited data. The volume, as usual, correlates tightly with generalization, while the flatness-generalization correlation is much more scattered, although it is slightly better than the correlation seen for the FCN on MNIST, and closer to the behaviour we observed for SGD in the main text.

G.2. More SGD-variant optimizers

In fig. S17 we provide further empirical results for the impact of choice of optimizer on the sharpness-generalization correlation by studying three common used SGD variants: Adagrad (Duchi et al., 2011), Momentum (Rumelhart et al., 1986) (momentum=0.9) and RMSProp (Tieleman & Hinton, 2012), as well as full batch gradient descent. Interestingly, full batch gradient descent (or simply gradient descent) shows behaviour that is quite similar to vanilla SGD. By contrast, for the other three optimizers, the correlation between sharpness and generalization breaks down, whereas the correlation between volume and generalization remains intact, much as was observed in the main text for Adam and Entropy-SGD. .

G.3. Larger training set

In order to rule out any potential training size effect on our main argument of the flatness, volume and generalization relationship, we further performed the experiments on MNIST with 10k training examples. Larger training sets are hard because of the GP-EP calculation of the volume scales badly with size. The results are shown in fig. S18. It is clear that the correlations between sharpness, volume and generalization follow the same pattern as we see in fig. 3, in which there are only $|S| = 500, |E| = 1000$ images. If anything, the correlation with volume is tighter.

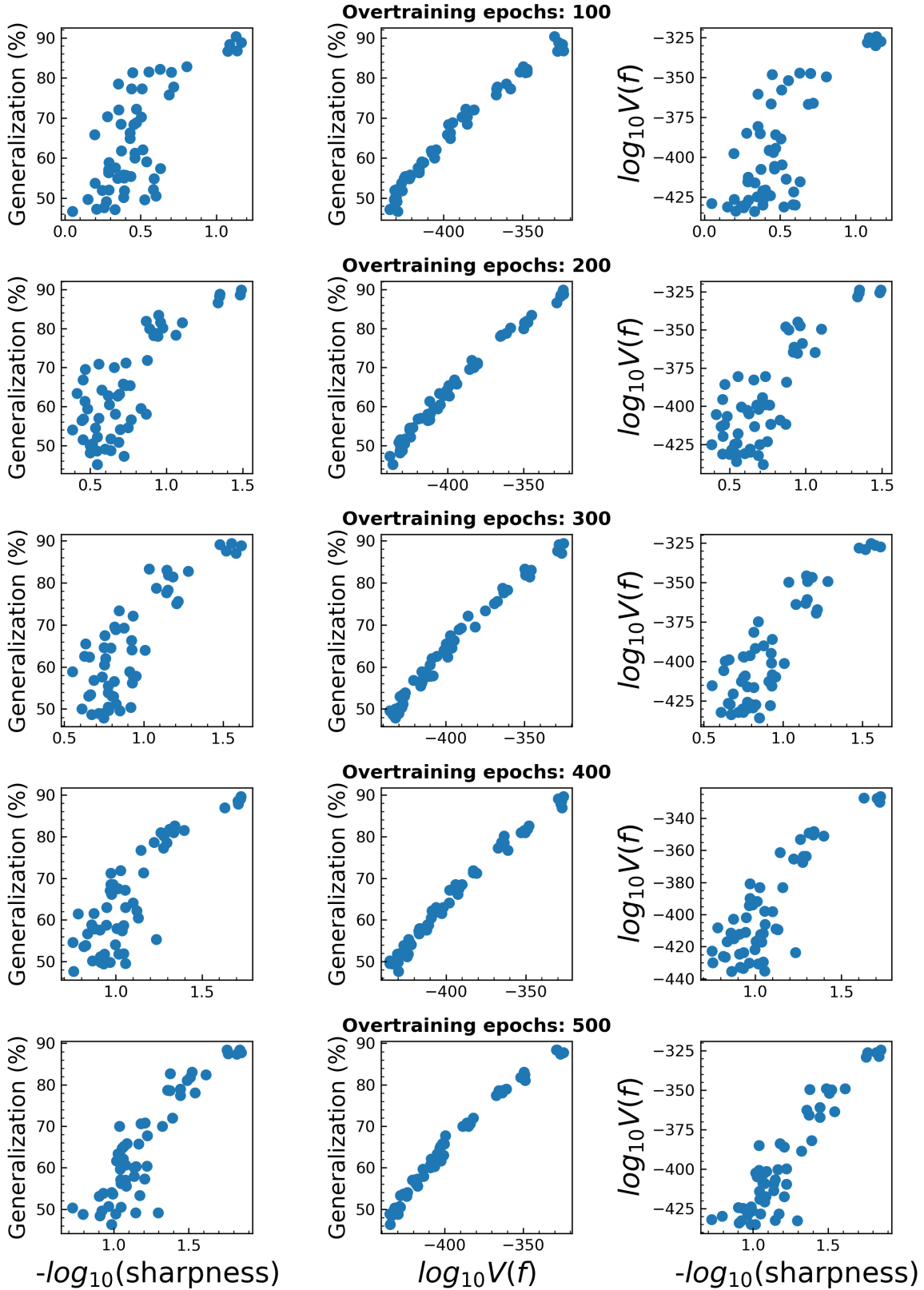


Figure S10. The correlation between sharpness, volume and generalization upon overtraining. The dataset is MNIST ($|S| = 500$, $|E| = 1000$), the optimizer is SGD. For the range of (100-500) overtraining epoch tested here, the overall values of sharpness drop with overtraining. By contrast, the volumes remain largely the same. For each quantity, the correlations remain remarkably similar with overtraining.

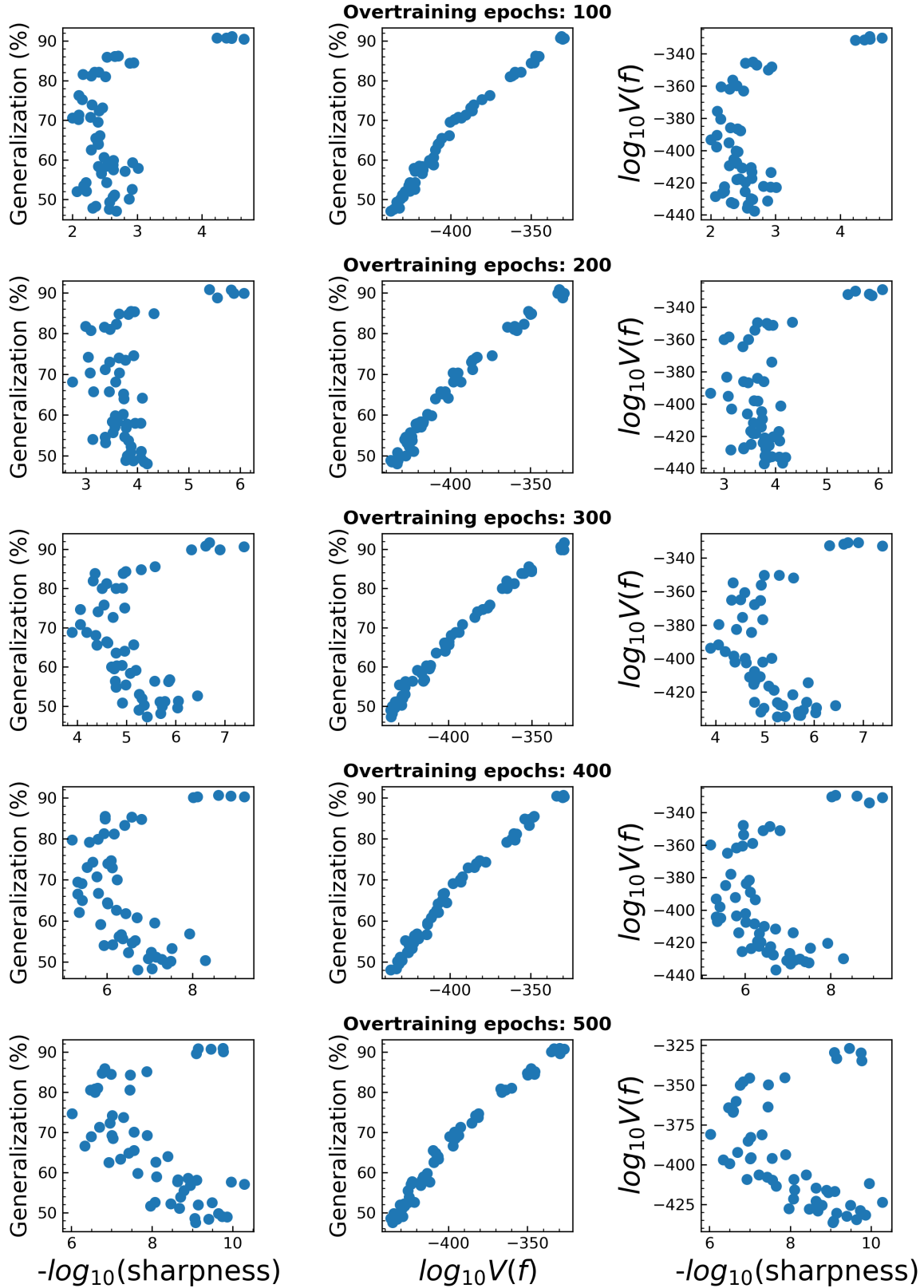


Figure S11. The correlation between sharpness, volume and generalization when over-trained (keep training after reaching zero training error). The dataset is MNIST ($|S| = 500$, $|E| = 1000$), the optimizer is Adam. The correlations are similar across different overtraining epochs.

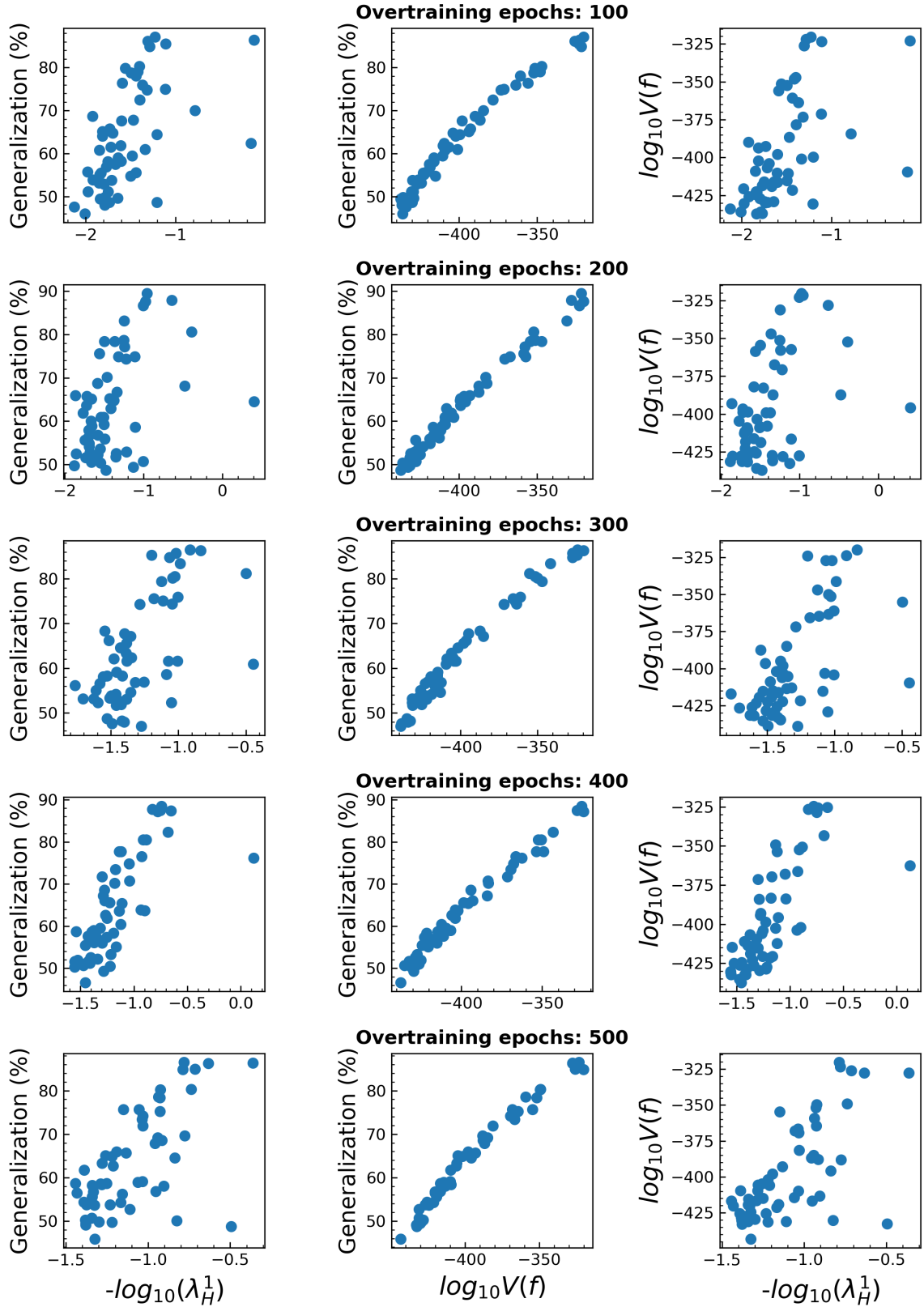


Figure S12. The correlation between Hessian spectral norm, volume and generalization when over-trained (keep training after reaching zero training error). The dataset is MNIST ($|S| = 500, |E| = 1000$), the optimizer is SGD. The correlations are similar across different overtraining epochs.

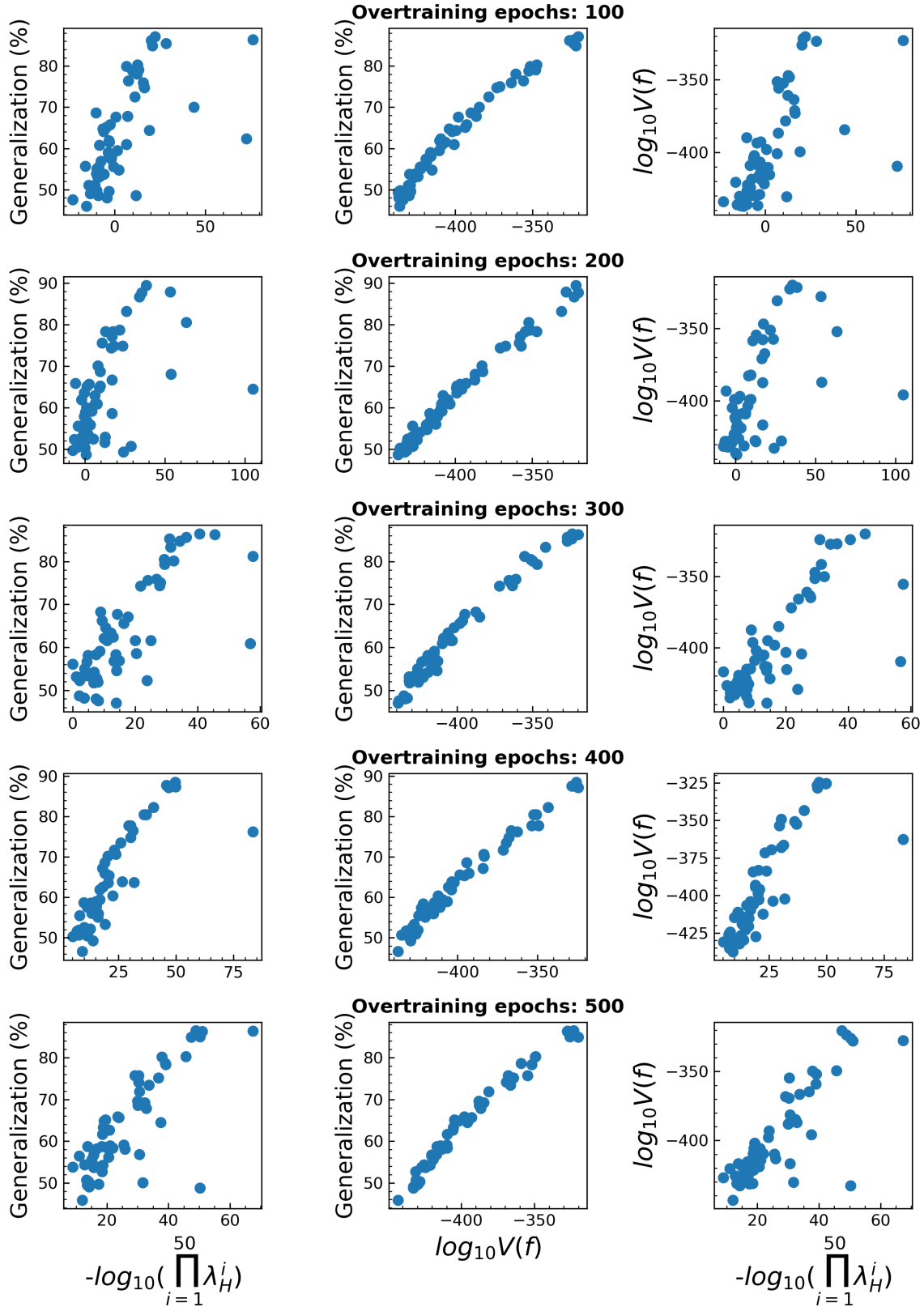


Figure S13. The correlation between Hessian based flatness (product of the top 50 largest Hessian eigenvalues), volume and generalization when over-trained (keep training after reaching zero training error). The dataset is MNIST ($|S| = 500$, $|E| = 1000$), the optimizer is SGD. The correlations are similar across different overtraining epochs.

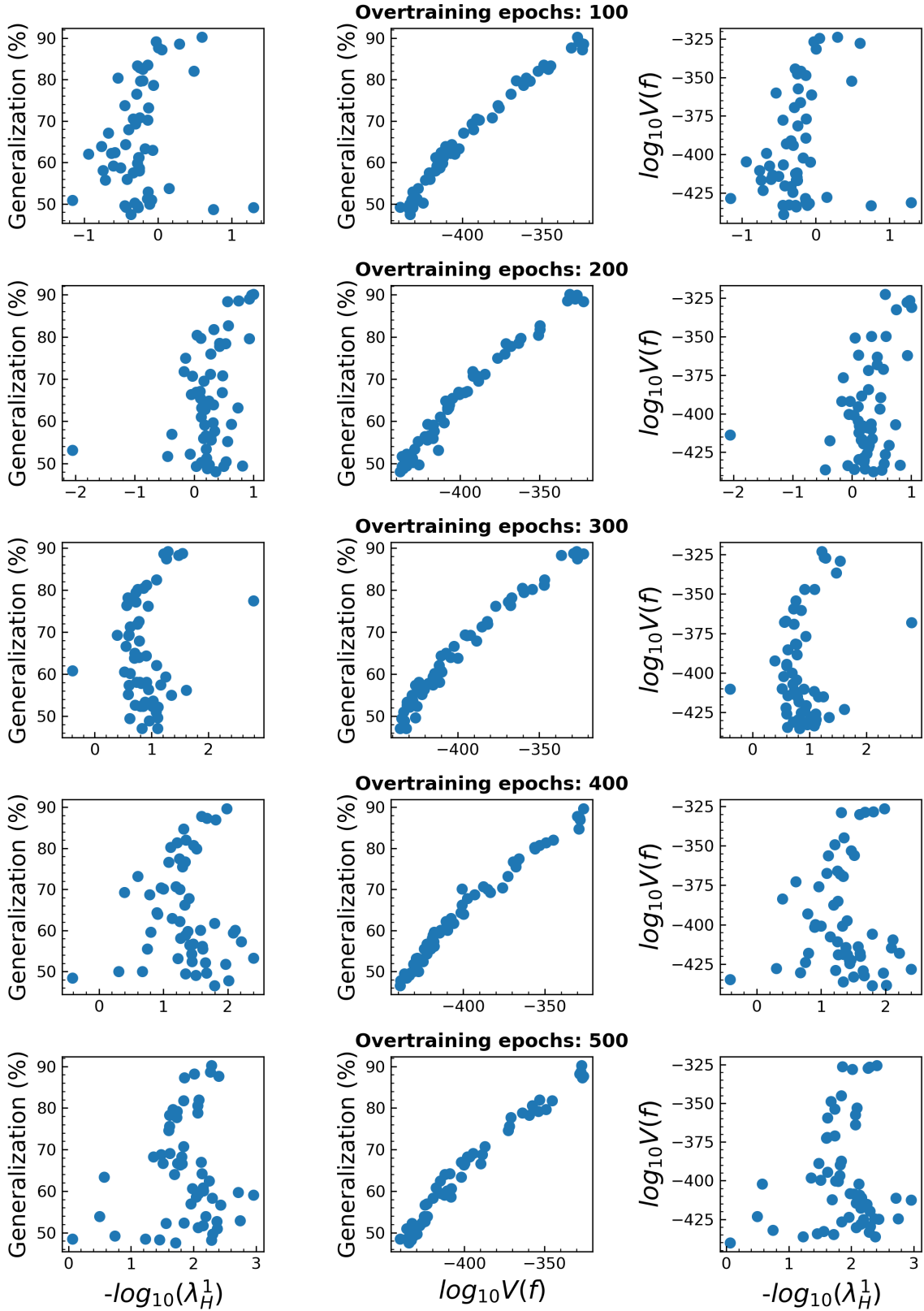


Figure S14. The correlation between Hessian spectral norm, volume and generalization when over-trained (keep training after reaching zero training error). The dataset is MNIST ($|S| = 500$, $|E| = 1000$), the optimizer is Adam. The correlations are similar across different overtraining epochs.

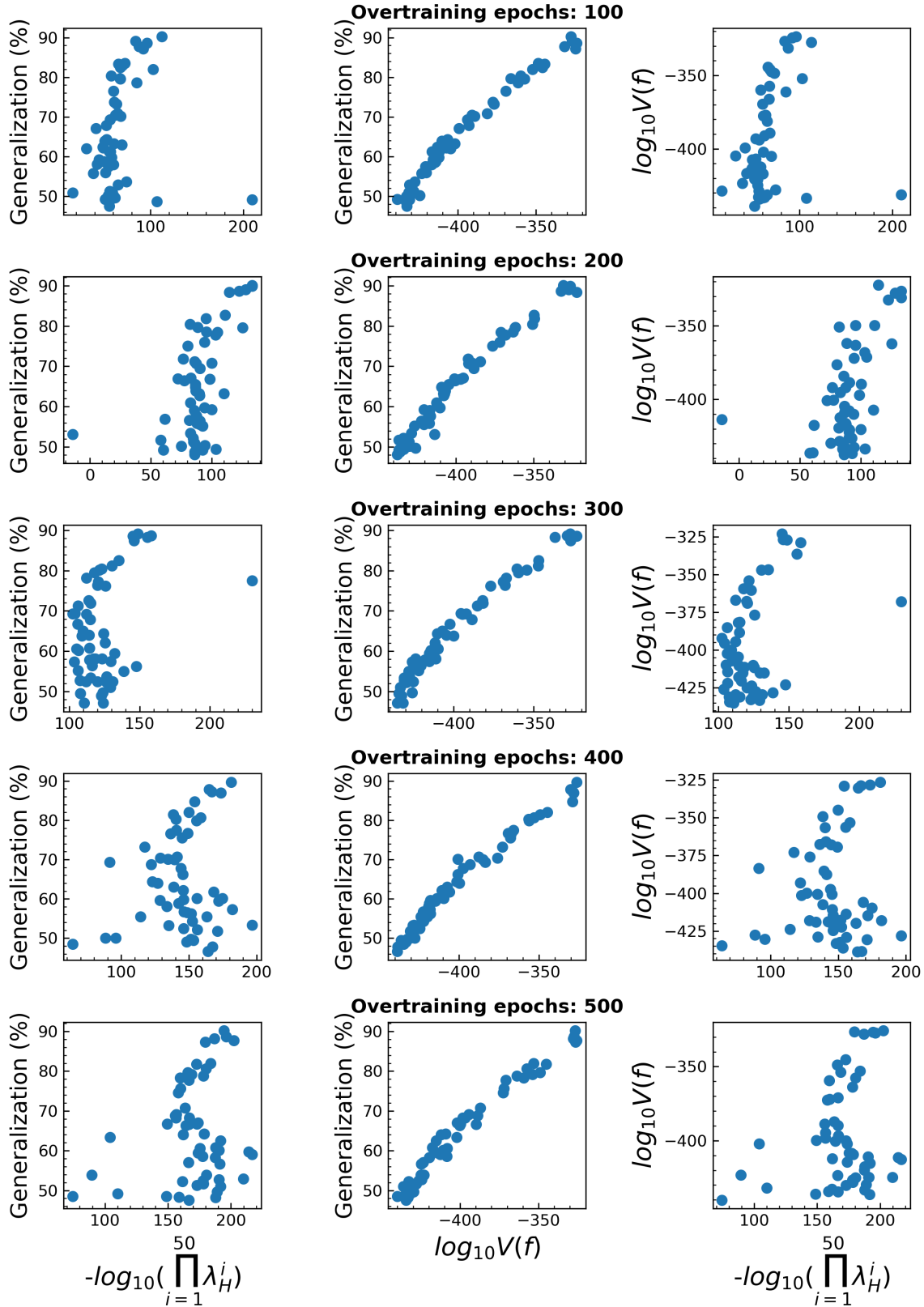


Figure S15. The correlation between Hessian based flatness (product of the top 50 largest Hessian eigenvalues), volume and generalization when over-trained (keep training after reaching zero training error). The dataset is MNIST ($|S| = 500$, $|E| = 1000$), the optimizer is Adam. The correlations are similar across different overtraining epochs.

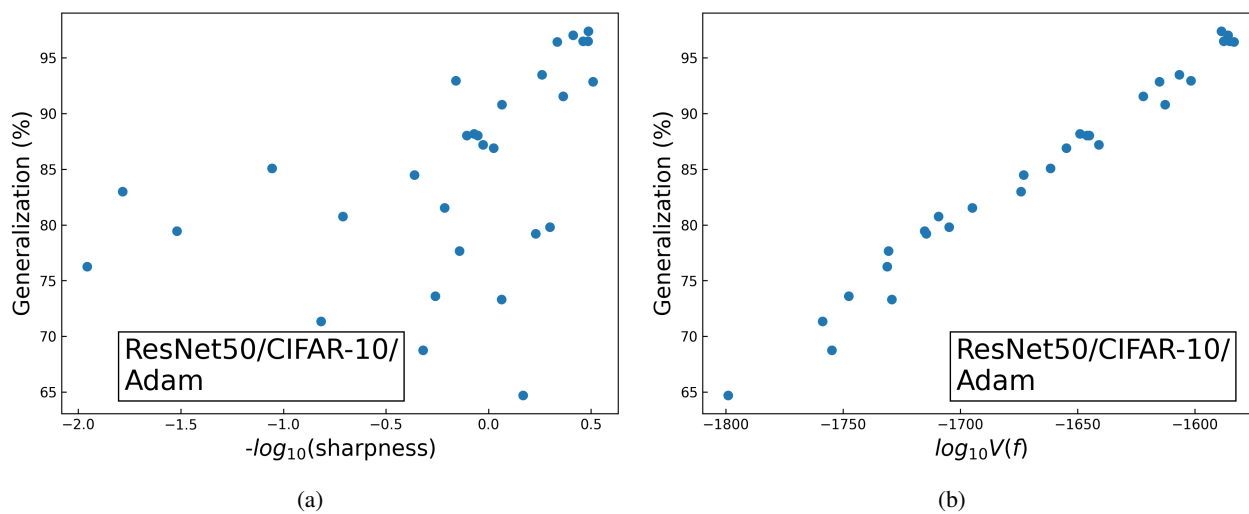


Figure S16. The correlation between generalization and (a) sharpness (b) volume for ResNet50 with $|S| = 5000$, $|E| = 2000$, and $|A|$ ranging from 0 to 2500, all on CIFAR-10.

WHY FLATNESS CORRELATES WITH GENERALIZATION FOR DEEP NEURAL NETWORKS

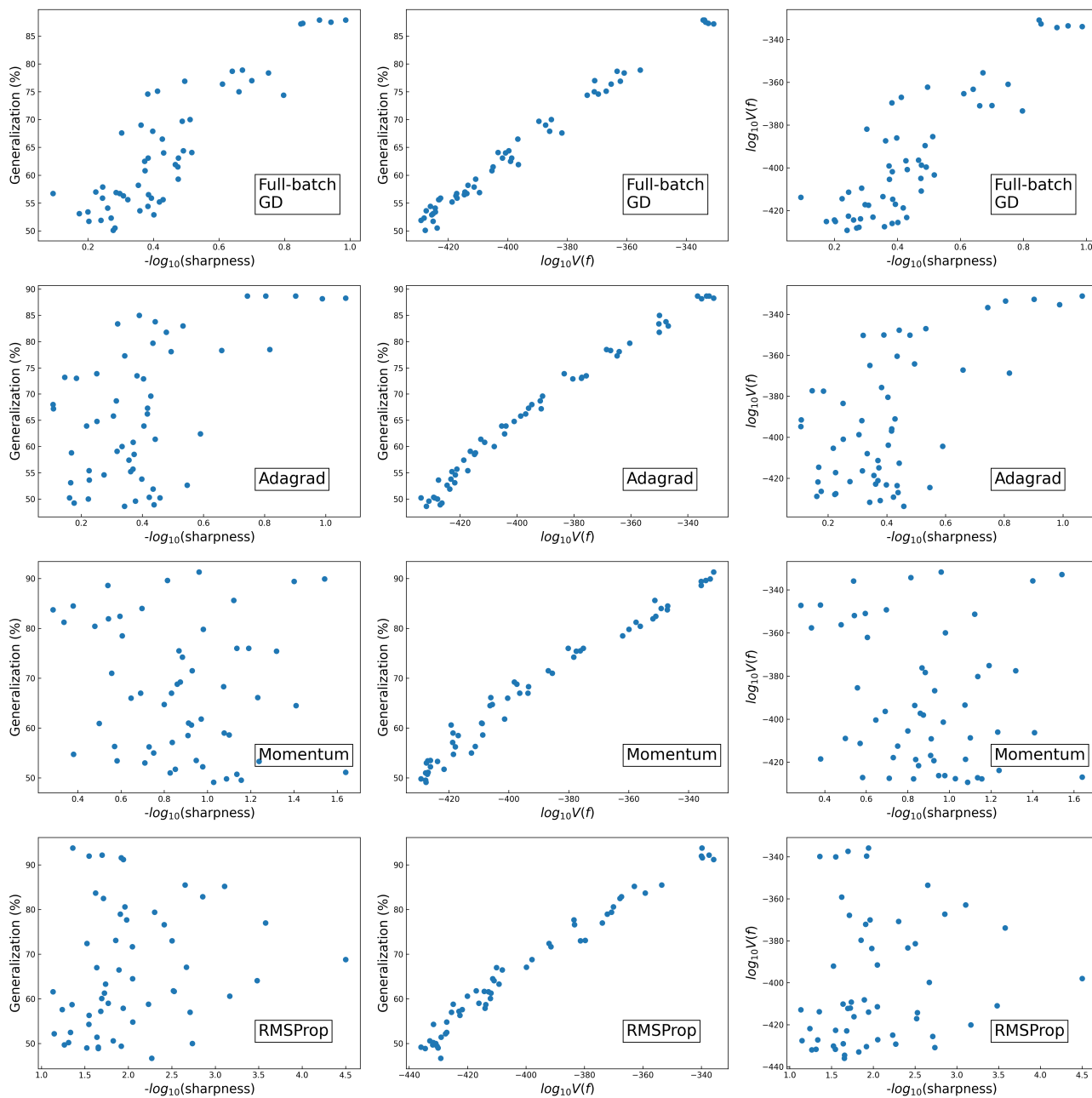


Figure S17. More results on the correlation between sharpness, volume and generalization when using other SGD-variant optimizers. The dataset is MNIST, $|S| = 500$, $|E| = 1000$. The architecture is FCN. The optimizers are full-batch gradient descent, Adagrad, Momentum (momentum=0.9) and RMSProp. All correlations are measured upon reaching zero training error.

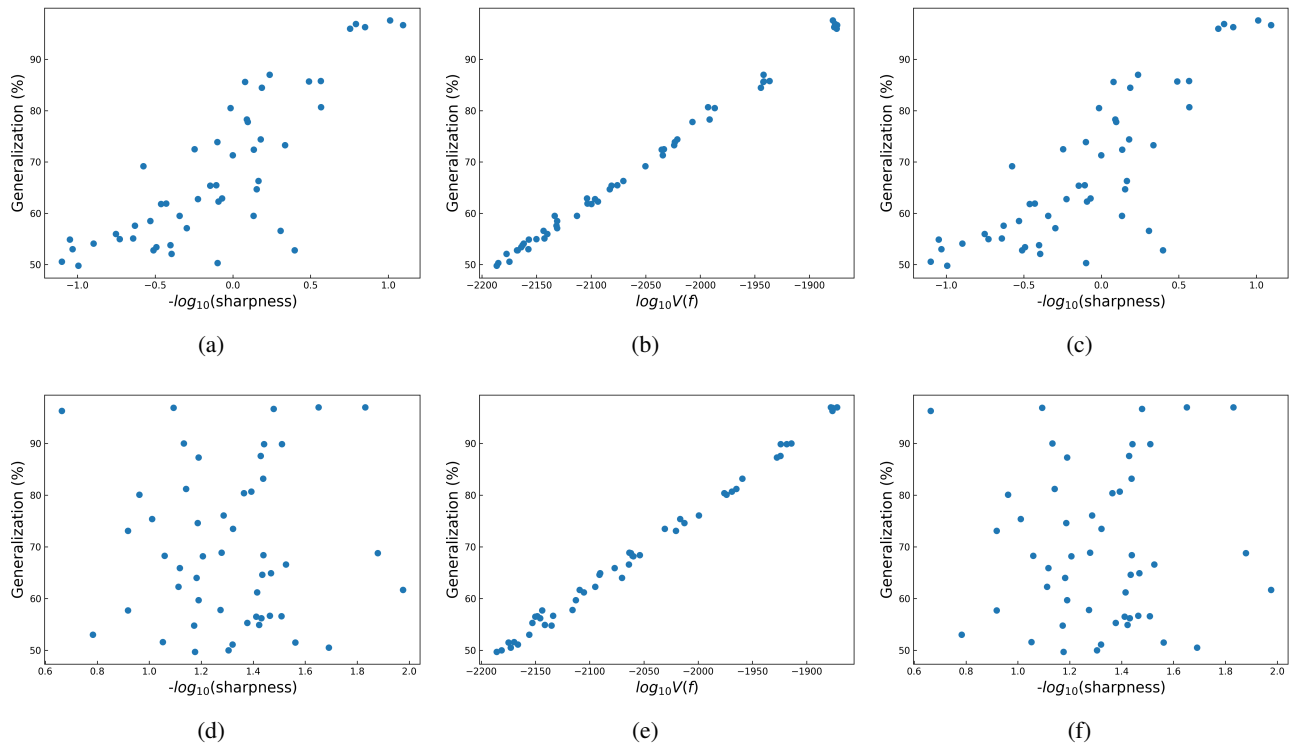


Figure S18. The correlation between sharpness, volume and generalization on MNIST with $|S| = 10000$, $|E| = 1000$. The attack set size ranges from 1000 to 9000. The architecture is FCN. (a)-(c): The FCN is trained with SGD; (d)-(f): The FCN is trained with Adam.